



University of Kentucky
UKnowledge

University of Kentucky Doctoral Dissertations

Graduate School

2001

POROSITY, PERCOLATION THRESHOLDS, AND WATER RETENTION BEHAVIOR OF RANDOM FRACTAL POROUS MEDIA

Michael C. Sukop

University of Kentucky, msukop@pop.uky.edu

[Right click to open a feedback form in a new tab to let us know how this document benefits you.](#)

Recommended Citation

Sukop, Michael C., "POROSITY, PERCOLATION THRESHOLDS, AND WATER RETENTION BEHAVIOR OF RANDOM FRACTAL POROUS MEDIA" (2001). *University of Kentucky Doctoral Dissertations*. 459.
https://uknowledge.uky.edu/gradschool_diss/459

This Dissertation is brought to you for free and open access by the Graduate School at UKnowledge. It has been accepted for inclusion in University of Kentucky Doctoral Dissertations by an authorized administrator of UKnowledge. For more information, please contact UKnowledge@lsv.uky.edu.

ABSTRACT OF DISSERTATION

Michael C. Sukop

The Graduate School
University of Kentucky

2001

POROSITY, PERCOLATION THRESHOLDS, AND WATER RETENTION
BEHAVIOR OF RANDOM FRACTAL POROUS MEDIA

ABSTRACT OF DISSERTATION

A dissertation submitted in partial fulfillment of the
Requirements for the Degree of Doctor of Philosophy
at the University of Kentucky

By

Michael C. Sukop

Co-Directors: Dr. Edmund Perfect, Assistant Professor of Agronomy
and Dr. John Grove, Associate Professor of Agronomy

Lexington, Kentucky

2001

ABSTRACT OF DISSERTATION

POROSITY, PERCOLATION THRESHOLDS, AND WATER RETENTION BEHAVIOR OF RANDOM FRACTAL POROUS MEDIA

Fractals are a relatively recent development in mathematics that show promise as a foundation for models of complex systems like natural porous media. One important issue that has not been thoroughly explored is the affect of different algorithms commonly used to generate random fractal porous media on their properties and processes within them. The heterogeneous method can lead to large, uncontrolled variations in porosity. It is proposed that use of the homogeneous algorithm might lead to more reproducible applications. Computer codes that will make it easier for researchers to experiment with fractal models are provided.

In Chapter 2, the application of percolation theory and fractal modeling to porous media are combined to investigate percolation in prefractal porous media. Percolation thresholds are estimated for the pore space of homogeneous random 2-dimensional prefractals as a function of the fractal scale invariance ratio b and iteration level i . Percolation in prefractals occurs through large pores connected by small pores. The thresholds increased beyond the 0.5927... porosity expected in Bernoulli (uncorrelated) networks. The

thresholds increase with both b (a finite size effect) and i . The results allow the prediction of the onset of percolation in models of prefractal porous media. Only a limited range of parameters has been explored, but extrapolations allow the critical fractal dimension to be estimated for many b and i values. Extrapolation to infinite iterations suggests there may be a critical fractal dimension of the solid at which the pore space percolates. The extrapolated value is close to 1.89 -- the well-known fractal dimension of percolation clusters in 2-dimensional Bernoulli networks.

The results of Chapters 1 and 2 are synthesized in an application to soil water retention in Chapter 3.

Keywords: Fractals, Porous Media, Percolation, Soil Water Retention

Michael C. Sukop

March 21, 2001

POROSITY, PERCOLATION THRESHOLDS,
AND WATER RETENTION BEHAVIOR
OF RANDOM FRACTAL POROUS MEDIA

By

Michael C. Sukop

Dr. Edmund Perfect
Co-Director of Dissertation

Dr. John Grove
Co-Director of Dissertation

Dr. John Grove
Director of Graduate Studies

March 21, 2001

RULES FOR THE USE OF DISSERTATIONS

Unpublished dissertations submitted for the Doctor's degree and deposited in the University of Kentucky Library are as a rule open for inspection, but are to be used only with due regard to the rights of the authors. Bibliographical references may be noted, but quotations or summaries of parts may be published only with the permission of the author, and with the usual scholarly acknowledgements.

Extensive copying or publication of the dissertation in whole or part also requires the consent of the Dean of the Graduate School of the University of Kentucky.

Name

Date

DISSERTATION

Michael C. Sukop

The Graduate School
University of Kentucky

2001

POROSITY, PERCOLATION THRESHOLDS,
AND WATER RETENTION BEHAVIOR
OF RANDOM FRACTAL POROUS MEDIA

DISSERTATION

A dissertation submitted in partial fulfillment of the
Requirements for the Degree of Doctor of Philosophy
at the University of Kentucky

By

Michael C. Sukop

Lexington, Kentucky

Co-Directors: Dr. Edmund Perfect, Assistant Professor of Agronomy
and Dr. John Grove, Associate Professor of Agronomy

Lexington, Kentucky

2001

Copyright by
Michael C. Sukop
2001

DEDICATION

This dissertation is dedicated to my youngest brother, Alexander Joseph Sukop, who passed away on December 14, 2000.

ACKNOWLEDGEMENTS

Partial funding for this work was provided by the University of Kentucky's Research Challenge Trust Fund and the University of Kentucky's Center for Computational Science.

N.R.A. Bird kindly provided the BASIC code used to produce the results in Bird and Dexter [1997]. The code was modified and used to generate the results in Chapter 3.

Gert Jaap van Dijk did a significant portion of the programming necessary to obtain the results in Chapter 2 and did the runs that resulted in Appendix C while a visiting scholar at the University of Kentucky.

I must thank my Father, Paul Sukop von Marko, who, in a complicated way, inspired me to finally return for the Ph.D. and who helped make it possible and tolerable in many other ways.

Many thanks are extended to my advisor Ed Perfect for his support in my quest to learn fractals and for providing stimulating interactions on essentially all of the technical content of the dissertation as well as in other areas in which we collaborated.

The faculty who served on my committee and as my teachers include Sergio Serrano, Craig Douglas, Scott Yost, M. Scott Smith, Mark Coyne, and John Grove. They deserve thanks for teaching me some new 'tricks', particularly with respect to software and mathematics, for being available for consultation, for teaching me about the academic world, and for providing a significant number of reference letters.

Gerald Haszler was lab technician and carried out the techniques we needed to do the significant number of solute transport column runs, as well as providing food and being an entertaining guy to hang out with.

Jim Thompson acted as sounding board on many issues, both technical and personal.

Jonathan Hu, Karen Walters, Danny Thorne, and Gundolf Hasse from the Math and Computer Science departments provided expert computer and mathematics help that helped me realize goals I might not have reached alone. It was not possible for me to reciprocate appropriately.

Finally, my friends Claire, Jim, Doug, Mark, Chad, the Jasons, Abigail, Cora, Nadege, and Carmen have all made my time in Kentucky more rewarding.

TABLE OF CONTENTS

Acknowledgements.....	iii
List of Tables	viii
List of Figures.....	ix
List of Files (for electronic version of Dissertation).....	xiii
Chapter 1. Homogeneous and Heterogeneous Fractal Algorithms for Pore-Scale	
Modeling of Porous Media	1
1.0 Summary.....	1
1.1 Introduction	1
1.2 Basic Prefractal Porous Media	2
1.2.1 Porosity	4
1.2.2 Lacunarity.....	4
1.3 Comparison of Algorithms for Generating Randomized Prefractal Porous Media... 8	
1.3.1 Homogeneous Algorithm	8
1.3.2 Heterogeneous Algorithm	9
1.4 Computer Codes	23
1.5 Conclusions	24
Chapter 2. Percolation Thresholds in 2-Dimensional Prefractal Models of Porous Media	
.....	25
2.0 Summary.....	25
2.1 Introduction	25
2.1.1 Percolation.....	25
2.1.3 Sierpiński Carpet as Percolation Cluster Model	29

2.1.4 Another perspective: Fractal Porous Media	31
2.1.5 Use of Fractal Dimension for Bernoulli Percolation.....	32
2.2 Literature Review	32
2.2.1 Percolation in Correlated Systems	32
2.2.2 Percolation on Fractals	33
2.3 Methodology.....	35
2.3.1 Hoshen-Kopelman Algorithm.....	35
2.3.2 Determination of Percolation Thresholds in Prefractals	35
2.3.3 Lattice Size and Finite-Size Scaling.....	38
2.3.4 Real Space Renormalization	41
2.3.5 Bounds on D_c	45
2.4 Results	47
2.4.1 Percolation Thresholds for Pore Space of Prefractals.....	47
2.4.2 Comparison with Uncorrelated Networks.....	53
2.4.3 Comparison with Dye Staining Images and Pore Networks from Thin Sections	54
2.5 Conclusions	56
Chapter 3. Application to Soil Water Retention.....	58
3.0 Summary.....	58
3.1 Previous Applications of Fractal Scaling to Soil Moisture Retention.....	58
3.2 Alternative Derivation of Fractal Water Retention Model.....	59
3.3 Three Parameter Model	63

3.4 Previous Work on Pore Connectivity and Coalescence in Fractal Water Retention	
Models	65
3.4 Conclusions	74
Appendices.....	75
Appendix A: Random Sierpiński Carpet Generator	75
Appendix B: Random Menger Sponge Generator.....	82
Appendix C: Porosity (ϕ), Standard Deviation of Porosity (σ), and Fractal Dimension (D) at the Percolation Threshold for Different Iteration Levels and Scale Invariance	
Ratios	88
References.....	91
Vita.....	99

List of Tables

Table 1. Nine realizations of 9 random numbers in $[0, 1]$. Values greater than $p = 8/9$ (pores) are underlined. N denotes the number of solids created by heterogeneous algorithm. ϕ is the porosity of the first-iteration structure. 10

Table 2. Binomial Probabilities for $p = 8/9$. These are effectively equivalent to the truncated binomial probabilities for this p value. 19

Table 3. Computation of Multifractal Spectrum for $p = 8/9$ 21

Table 4. Maximum Lattice Sizes 41

Table 5. Regression equations, number of points regressed (n) and coefficients of determination (r^2) for extrapolations to infinite iteration levels (Figure 23). 52

Table 6. Ratio of interquartile ranges of saturation for heterogeneous and homogeneous algorithms at each tension for varying p . ($3^{\text{rd}}-1^{\text{st}}$ quartiles heterogeneous/ $3^{\text{rd}}-1^{\text{st}}$ quartiles homogeneous). 73

List of Figures

Figure 1. Sierpiński Carpet constructed to fourth iteration level (Solids white, voids black).....	3
Figure 2. Three $i = 3$, $b = 7$, $D = \log 40/\log 7$ prefractals illustrating low (A), intermediate (B), and high (C) degrees of pore coalescence or lacunarity (Solids white, voids black).....	5
Figure 3. Semivariograms for low, intermediate, and high lacunarity pre-fractals of Figure 2 and for the mean of 10 randomized variants ($i = 3$, $b = 7$, $D = \log 40/\log 7$). Error bars indicate +/- 1 standard deviation from mean.	7
Figure 4. Randomized Sierpiński Carpet constructed to fourth iteration level with homogeneous algorithm. Note that the number of pores of each size class (neglecting coalescence) is in strict agreement with the number in the standard Sierpiński carpet (Figure 1).	9
Figure 5. Randomized Sierpiński Carpet constructed to fourth iteration level with heterogeneous algorithm. Note that the number of pores of each size class does not agree with the number in the standard Sierpiński carpet (Figure 1) or the randomized carpet in Figure 4.	11
Figure 6. Menger sponge, homogeneous and heterogeneous randomized variants.....	11
Figure 7. Binomial, truncated binomial, uniform, and Dirac distributions of the number of solids as a function of p	13
Figure 8. Distributions of porosity for 1000 realizations of homogeneous and heterogeneous algorithms at $p = 8/9$ and $p = 6/9$ with $b = 3$, $i = 5$	15

Figure 9. Multifractal spectra for 2-dimensional Sierpiński carpets with $p = 1/9, 2/9, \dots, 8/9$. Spectrum for uniform distribution also shown.	23
Figure 10. Connectivity to top boundary as a function of pore probability. Solids black, pores unconnected to top boundary white, pores connected to top boundary red or gray.	27
Figure 11. Comparison between percolation cluster in Bernoullian lattice (1024 x 1024) at p_c with randomized Sierpiński carpet ($b = 3, N = 8, i = 6$). Percolation cluster measured $D = 1.839\dots$, Randomized carpet $D = 1.892\dots$	30
Figure 12. Lin and Yang [1997] approach to percolation on fractal set problem. Conducting solids black, non-conducting solids gray, and pores white.	34
Figure 13. Hoshen-Kopelman algorithm.	35
Figure 14. Fitted cumulative normal distributions for $b = 3$ and $i = 1$. Theoretical and empirical percolation probabilities.	37
Figure 15. Percolation thresholds plus or minus the standard deviations for the first iteration level.	38
Figure 16. Finite-size effect for $i = 1$ results.	39
Figure 17. Renormalization for square site network. Gray sites occupied.	42
Figure 18. Mandelbrot's [1983] bounds and Perreau et al's [1996] renormalization results for percolation of the solids.	46
Figure 19. Maximum number of pores without pore percolation; Solids black, pores white.	47
Figure 20. Percolation in the pore space of a randomized Sierpiński carpet with $b = 10, N = 63$, and $i = 3$ ($D = 1.799\dots$). Note that percolation in the large pores depends on	

the small pores. Solids black, pores connected to upper boundary that form a sample spanning cluster red, other pores white.....	48
Figure 21. Upper and Lower Bounds on D_c for percolation as a function of the scale invariance ratio b and empirical results.	49
Figure 22. Fractal Dimension D as a function of b and i for 50% porosity Menger sponge.	50
Figure 23. Relationship between D_c and inverse iteration level for different scale invariance ratios.	51
Figure 24. Empirical results (circles) and computation assuming no effect of network spatial correlation (solid lines and crosses).	54
Figure 25. Comparison of a portion of a soil dye-staining image (top left; approximately 40x40 cm, Costa Rican ultisol ; Schwartz et al., 1999; $D = 1.79$), thin section image (top right) [Ringrose-Voase, 1987], Bernoullian percolation cluster (bottom left; $D = 1.839\dots$), and percolation cluster in fractal porous medium (bottom right; porous medium $D = 1.799\dots$).	56
Figure 26. Perfect [1999] model for soil water retention in fractal pore space.	65
Figure 27. Impact of different algorithms on simulated water retention: (A) homogeneous, $p=8/9$, (B) Heterogeneous, $p=0.9$. Heterogeneous results from Bird and Dexter [1997], Figure 3.....	67
Figure 28. Impact of different algorithms on simulated water retention: (A) homogeneous, $p=7/9$, (B) heterogeneous, $p=0.8$. Heterogeneous results from Bird and Dexter [1997], Figure 3.....	69

Figure 29. Impact of different algorithms on simulated water retention: (A) homogeneous, $p=6/9$, (B) heterogeneous, $p=0.7$. Heterogeneous results from Bird and Dexter [1997], Figure 3..... 70

Figure 30. Impact of homogeneous and heterogeneous fractal-generating algorithms on simulated water retention for 1000 realizations of 2-dimensional $b = 3$, $i = 5$ prefactal porous media with $p=8/9$ 71

Figure 31. Impact of homogeneous and heterogeneous fractal-generating algorithms on simulated water retention for 1000 realizations of 2-dimensional $b = 3$, $i = 5$ prefactal porous media with $p=7/9$ 72

Figure 32. Impact of homogeneous and heterogeneous fractal-generating algorithms on simulated water retention for 1000 realizations of 2-dimensional $b = 3$, $i = 5$ prefactal porous media with $p=6/9$ 72

List of Files (for electronic version of Dissertation)

File name: Sukopdis.pdf

File size: 1.14 MB

Chapter 1. Homogeneous and Heterogeneous Fractal Algorithms for Pore-Scale Modeling of Porous Media

1.0 Summary

Fractal models of porous media are of interest in numerous scientific disciplines, including hydrology, petroleum engineering, and soil science. This interest arises from the ability of these models to parsimoniously produce highly complex and richly structured geometries. Examination of the soil hydrology literature suggests that there are at least two different ways these models are being constructed. One of these methods results in a type of multifractal behavior that can lead to large, uncontrolled variations in porosity. The methods are reviewed here and it is proposed that use of the 'homogeneous' algorithm might lead to more reproducible and fruitful applications. Computer codes that will make it easier for more researchers to experiment with fractal models are provided.

1.1 Introduction

Fractal models of porous media are enjoying considerable popularity (eg., Adler and Thovert, 1993; Perrier et al., 1995; Bird and Dexter, 1997; Rieu and Perrier, 1998; Crawford et al., 1999; Perrier et al., 1999; Rappoldt and Crawford, 1999). This is due in part to the relatively small number of parameters that can define a random fractal porous medium of great complexity and rich structure. Also, fractal scaling of natural porous media has been widely anticipated on the basis of the observed power law form of soil water retention curves [Ahl and Niemeyer, 1989; Tyler and Wheatcraft, 1990; Rieu and Sposito, 1991a, b, c; Perrier et al., 1996; Perfect, 1999]. There has been considerable debate about the usefulness of the approaches presented in these papers because they generally neglect pore connectivity [Bird, et al., 1996; Rieu and Perrier, 1998]. One way that this limitation can be surmounted is to compute retention in simulated realizations of known fractal porous media [Perrier et al., 1995; Bird and Dexter, 1997; Stepanek et al., 1999]. Similarly, other processes of interest, for example, gas transport in soils [Rappoldt

and Crawford, 1999; Crawford et al., 1993], solute transport [Adler and Thovert, 1993], and microbial dynamics [Crawford et al., 1993] can be usefully studied in simulated fractal porous media. As such simulations become more widespread, it is valuable to examine the methods used to generate the fractal porous media and the properties of the simulated media.

Various modifications of basic fractal-generating algorithms, such as assemblages of fractal 'patches' or fractal cell arrays [Bird and Dexter, 1997; Rappoldt and Crawford, 1999] and pore-solid fractals [Perrier et al., 1999] have been proposed and applied. Saucier and Muller [1993] and Muller [1996] have also applied multifractal approaches to porous media. The focus here however is on the most basic models, and these variants are not addressed further except in relation to the implications of the 'patch' approach for porosity and the multifractal artifacts that arise with a particular algorithm. Rieu and Perrier [1998] make the distinction between 'mass' and 'pore' fractal models. Only mass fractal models are considered here, though the issues addressed apply equally to random pore fractal models. Fundamental fractal scaling requirements are reviewed and different fractal-generating algorithms are contrasted. In particular, problems that arise in the application of a particular algorithm are demonstrated.

1.2 Basic Prefractal Porous Media

The fractals we consider first are scale-invariant constructions that follow simple number-size relations. Porous fractals are often constructed from a solid starting mass by an iterative process of mass removal and re-scaling. As a concrete example, we consider the perhaps familiar Sierpiński carpet, which has $E = 2$ (the embedding or Euclidian dimension), $b = 3$ (a scale reduction factor), and $p = 8/9$ (the probability of a solid at any iteration level) (Figure 1).

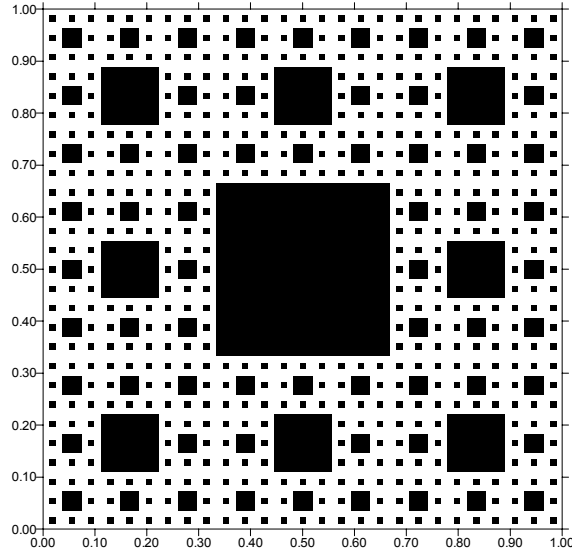


Figure 1. Sierpiński Carpet constructed to fourth iteration level (Solids white, voids black).

Construction begins with a solid square of size 1 x 1 from which 1 square area of size 1/3 by 1/3 is removed from the center. N is the number of solids of the new size remaining at any iteration level (for our example, $N = 8$ for the first iteration) and r is the linear measure of a pore or solid. Note that r depends on b as $r = (1/b)^i$ where i is the iteration level. In a fractal of unit side length, $N = r^{-D}$, and the ratio $-\log N / \log r$ gives the mass fractal dimension D . As is generally true for such ratios, point estimates based on individual pairs of N and r or slope estimates based on numerous pairs can be computed. For the standard Sierpiński carpet, $N = 8$ and $r = 1/3$ at the first iteration level. Hence, on the basis of this pair of N and r , $D = -\log(8) / \log(1/3) = 1.89\dots$. At the second iteration $N = 64$ and $r = 1/9$. Therefore, $D = -\log(64) / \log(1/9) = 1.89\dots$. Computation of the double logarithmic slope between the points leads to

$$D = -\frac{d \log N}{d \log r} = -\frac{\Delta \log N}{\Delta \log r} = -\frac{\log 8 - \log 64}{\log 1/3 - \log 1/9} = 1.89\dots \quad (1)$$

We recover the exact fractal dimension from either procedure.

1.2.1 Porosity

The porosity (ϕ) of a 'true' fractal (in which the generating process is iterated an infinite number of times) is always unity. Hence, such models are of little use as models of natural porous media such as soil, aquifer, or reservoir material. However, by introducing a lower 'cutoff' size, where the generating process ceases, we can maintain a realistic porosity. Thus, we can define such a 'prefractal' [Feder, 1988] in terms of any three of the following four parameters: D , b , i , and ϕ (or p). Equation (2) expresses the relationship between these parameters in terms of the total porosity for a prefractal embedded in E -dimensional space:

$$\phi = 1 - \frac{N}{b^{Ei}} = 1 - \frac{b^{Di}}{b^{Ei}} = 1 - b^{i(D-E)} \quad (2)$$

Depending on the iteration level, we also have:

$$\phi = (1 - p) + (1 - p)p + (1 - p)p^2 + \dots \quad (3)$$

In general, for $i \geq 2$,

$$\phi = (1 - p) \left[\left(\sum_{j=1}^{i-1} p^j \right) + 1 \right], \quad (4)$$

which can be simplified to

$$\phi = 1 - p^i. \quad (5)$$

Equation (5) works for any iteration level $i > 0$.

1.2.2 Lacunarity

It is necessary to consider one additional parameter for completeness, though its effect is not expected to be significant for the randomized prefRACTALS that we consider next. The additional parameter is related to the coalescence of pores. Figure 2 shows three 2-dimensional porous structures that have identical mass fractal dimensions and porosities and yet exhibit extreme differences in their pore arrangements.

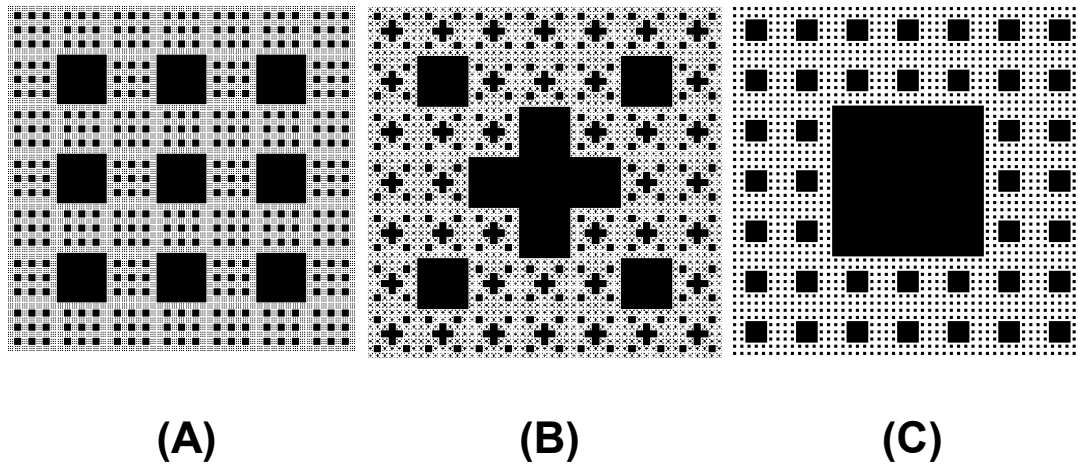


Figure 2. Three $i = 3$, $b = 7$, $D = \log 40/\log 7$ prefRACTALS illustrating low (A), intermediate (B), and high (C) degrees of pore coalescence or lacunarity (Solids white, voids black).

Figure 2A represents a condition in which the pores are maximally dispersed. The nine largest pores (and so on at each iteration level) of Figure 2A are coalesced into one large pore in Figure 2C. Figure 2B has an intermediate degree of pore coalescence. In the fractal literature, this phenomenon is described by the lacunarity. Highly lacunar fractals have large gaps as a result of pore coalescence. Several measures of lacunarity have been proposed. Many of these relate to the degree of translational invariance that the fractal displays. For example, the structure in Figure 2A can be translated $2/7$ units in the x or y directions and will exactly overlies its own pores. No such translation is possible for the structures in Figures Figure 2B and Figure 2C.

Here we apply spatial autocorrelation as a measure of lacunarity. The spatial autocorrelation is closely related to the translational invariance [Gouyet, 1996]. The semivariogram measures the spatial autocorrelation and is computed as

$$\gamma(h) = \frac{1}{2n} \sum (z_x - z_{x+h})^2 \quad (6)$$

γ is the semivariance, h is the separation distance or lag between points at x and $x + h$, n is the number of points separated by h , and z is the value of the property under study. The summation is taken over all n pairs of points separated by h . In our case, z is a single binary digit 0 or 1 representing a pore or solid respectively and hence the variogram is known as an indicator variogram. The semivariance can also be computed in specific directions, but all directions are treated equally here.

The variogram plots the lag on the abscissa against the semivariance on the ordinate. At small lags (short separation distance), the values z are more likely to be close to one another and a small semivariance is often observed. At larger separation distances, the spatial autocorrelation decreases and the semivariance value increases to the variance of the entire data set. The separation distance or lag at which this occurs is known as the range of spatial autocorrelation.

Figure 3 shows the semivariograms of the structures in Figure 2 and a randomized (see below) variant. The variograms are omnidirectional, 2-dimensional, indicator variograms for the entire image presented in Figures Figure 2A, Figure 2B, and Figure 2C. Lag is expressed relative to the image size. The interpretation proposed here for the significance of the ranges of the spatial autocorrelations observed for the *known* low, intermediate, and high lacunarity structures of Figure 2 (short, intermediate, and long range respectively) is exceedingly simple: there is a direct correspondence between the lacunarity and the range.

The semivariogram for the intermediate lacunarity structure (Figure 2B) and the randomized variant are similar. These curves are much smoother and generally fall between the curves for the high- and low-lacunarity prefractals. Moreover, the range of

spatial autocorrelation (where the semivariograms first intersect the variance) is short for the low lacunarity prefractal, long for the high lacunarity prefractal, and intermediate and indistinguishable for the intermediate and random prefractals. It is very important to note that the irregular-looking curves for the high and low lacunarity cases are not the product of any random process but rather are the result of a well-defined measurement (the variogram) on completely deterministic structures. They are completely reproducible and exact: there is no variability about the variogram estimates.

The similarity between the variograms for the intermediate lacunarity structure and the randomized structure suggests that potential difficulties associated with lacunarity as an additional variable as it is manifested in these contrived examples are eliminated by randomization. This shows (and this has not been expressed in the previous literature on fractal porous media models) that for the randomized models created here, we can safely disregard the lacunarity. Ultimately, it may be desirable to develop random prefractal models in which the lacunarity can be explicitly controlled. The work of Nauman [1993] might readily be adapted to such an effort.

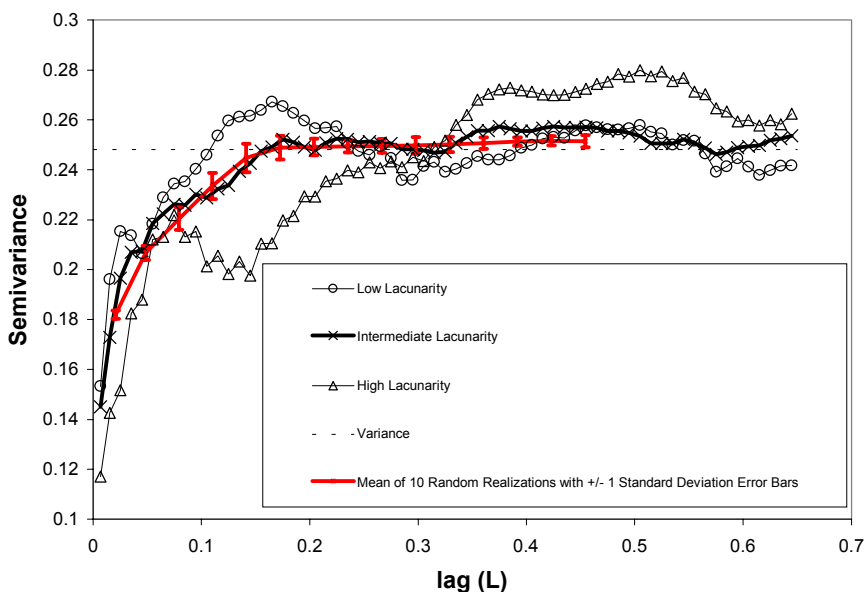


Figure 3. Semivariograms for low, intermediate, and high lacunarity pre-fractals of Figure 2 and for the mean of 10 randomized variants ($i = 3$, $b = 7$, $D = \log 40/\log 7$). Error bars indicate ± 1 standard deviation from mean.

1.3 Comparison of Algorithms for Generating Randomized Prefractal Porous Media

1.3.1 Homogeneous Algorithm

Clearly, the prefractals in Figure 1 and Figure 2 bear little resemblance to natural porous media like soils and aquifer or reservoir materials because of their regularity and lack of pore connectivity. Now the question arises, "How are we to construct a randomized version of a prefractal?". One method that maintains strict adherence to the fractal scaling law, $N = r^{-D}$, and therefore returns the correct fractal dimension using both the individual point ratios, $\log(N)/\log(1/r)$, and the slope measures, is to assign a random permutation of the integers 1 through b^E to each site of a lattice and then make those with an integer value $j \leq p b^E$ solids. Iterating this algorithm produces prefractal porous media that can be classified as homogeneous [Gouyet, 1996]. This approach has also been called 'constrained' [Mandelbrot, 1983] and 'microcanonical' curdling [Mandelbrot, 1974].

For the classical Sierpiński carpet, $1 \leq j \leq 9$, $p = 8/9$, $b = 3$, and $E = 2$. Hence, sites with $j \leq 8/9 \cdot 3^2$ (i.e., $j \leq 8$) are retained as solids. For the second iteration, the same algorithm is applied independently to each of the 8 solids that remain, and so on for subsequent iterations. Figure 4 shows the results of the application of this algorithm. If we neglect the coalescence of adjacent pores, there is exactly one large pore (and hence 8 solids) at the first iteration level and there are exactly 8 pores at the second iteration level. Pore coalescence does not affect the total porosity but may be of significance for example in the study of water retention.

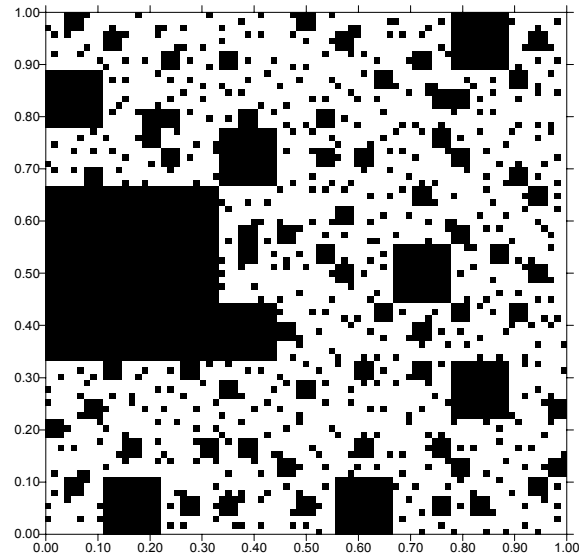


Figure 4. Randomized Sierpiński Carpet constructed to fourth iteration level with homogeneous algorithm. Note that the number of pores of each size class (neglecting coalescence) is in strict agreement with the number in the standard Sierpiński carpet (Figure 1).

1.3.2 Heterogeneous Algorithm

Bird and Dexter [1997] and Rappoldt and Crawford [1999] present random prefractal models of porous media. In both cases, some of these prefractals were constructed using an algorithm that can be summarized as follows:

- Choose a probability p that a site is a solid;
- For each site in a space divided into b^E sites (where E is the Euclidian embedding dimension 1, 2, or 3), generate a uniformly distributed random number in the interval $[0,1]$;
- If the random number is greater than p , make the site a pore.

Mandelbrot [1974, 1983] calls this canonical curdling while Gouyet [1996] identifies it as a random heterogeneous fractal. Let us consider the behavior of this algorithm. Say that we wish to generate a randomized Sierpiński carpet. Hence $p = 8/9$ ($=0.888\dots$). We generate 9 realizations of $b^E = 9$ random numbers and show them in Table 1. It is clear from Table 1 that the heterogeneous algorithm often fails to return the number of solids (8 for the Sierpiński carpet) needed to satisfy the simple fractal scaling law $N = r^{-D}$. For

the first realization on the first line, $N = 7$ and $r = 1/3$. Hence, the fractal dimension based on the point estimate is $D = -\log(7)/\log(1/3) = 1.77\dots$ rather than $D = 1.89\dots$ as is characteristic of the classical Sierpiński carpet (Figure 1).

Table 1. Nine realizations of 9 random numbers in $[0, 1]$. Values greater than $p = 8/9$ (pores) are underlined. N denotes the number of solids created by heterogeneous algorithm. ϕ is the porosity of the first-iteration structure.

Realization	Random numbers in $[0, 1]$									N	ϕ
1	0.8712	0.606	0.2482	0.4722	0.566	<u>0.9357</u>	0.3504	<u>0.9946</u>	0.0136	7	0.22...
2	0.5845	0.8111	<u>0.9886</u>	0.7324	0.7607	0.6739	0.613	0.8774	0.7895	8	0.11...
3	0.6026	0.4618	0.5643	<u>0.9806</u>	0.3452	0.4279	0.3377	0.6259	<u>0.8996</u>	7	0.22...
4	0.4882	0.0937	0.2205	0.6668	0.4475	0.8328	0.636	0.2119	0.0022	9	0
5	<u>0.9426</u>	0.1027	0.8775	0.6831	0.5158	0.1713	0.5166	<u>0.9155</u>	0.5163	7	0.22...
6	0.3465	0.8745	0.7276	0.8754	0.1573	0.4406	0.5195	0.1343	0.6244	9	0
7	0.1997	0.0608	0.8531	0.5077	<u>0.9809</u>	0.7524	0.6264	<u>0.9681</u>	0.2652	7	0.22...
8	0.0981	0.8472	0.1777	0.4679	0.2988	0.6155	<u>0.9492</u>	0.6199	0.399	8	0.11...
9	0.6521	0.4541	0.5403	0.2448	0.1546	0.2542	0.2235	0.6408	<u>0.9776</u>	8	0.11...

Figure 5 shows a randomized Sierpiński carpet based on the heterogeneous algorithm. In this realization, there are no pores at the first iteration level (like Realization 4 of Table 1), and only six (again ignoring pore coalescence) at the second level. The point estimates of the fractal dimension are 2.000, 1.965, 1.945, and 1.933 for the first, second, third, and fourth iterations respectively. The slope estimate of D is 1.9096 and is close to the true value; this is because double logarithmic slope estimates of D are typically relatively resistant to variations in the number of solids.

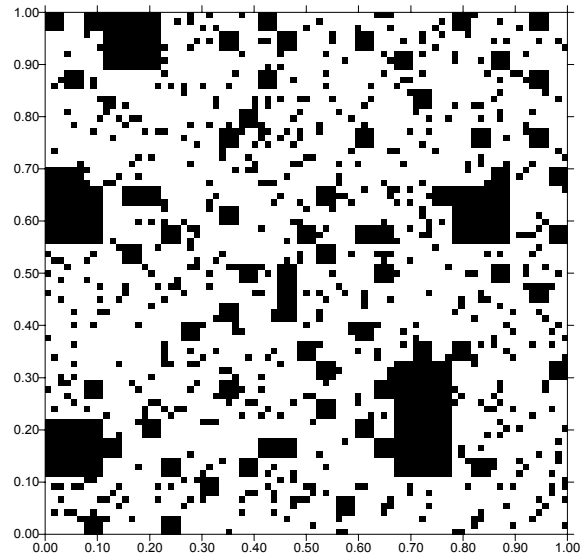


Figure 5. Randomized Sierpiński Carpet constructed to fourth iteration level with heterogeneous algorithm. Note that the number of pores of each size class does not agree with the number in the standard Sierpiński carpet (Figure 1) or the randomized carpet in Figure 4.

The same behavior occurs in the 3-dimensional case. Figure 6 shows the Menger sponge, and homogeneous and heterogeneous random analogues.

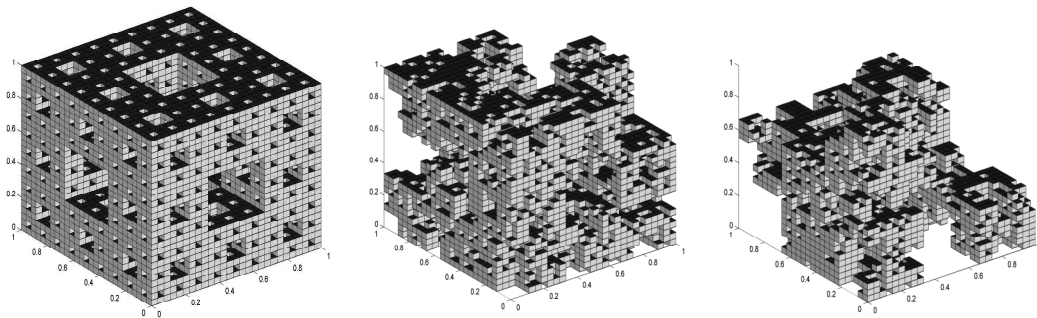


Figure 6. Menger sponge, homogeneous and heterogeneous randomized variants.

It is interesting to note that several publications [Crawford, 1994; Crawford and Young, 1998] appear to describe the approach used to generate prefractal Sierpiński carpet structures in terms of the heterogeneous algorithm and display figures that are almost certainly generated with a homogeneous algorithm. This fosters little appreciation for the

differences between the algorithms and the porosity implications that we demonstrate here.

The implications for the porosity of structures generated using the heterogeneous algorithm are particularly significant. The areal porosity of the first iteration of a Sierpiński carpet is $1/9$. The areal porosities of the first iteration structures generated using the values in Table 1 can range from 0 to $2/9$, or from non-porous to twice the expected porosity. In only three of nine cases is the porosity equal to the expected value.

As an expansion of the results in Table 1, Figure 7 shows the analytical distributions of the number of solids as a function of p . The reason for the asymmetry in Figure 7 (and for the fundamentally different character of the heterogeneous algorithm) is that the results follow binomial distributions. It appears that this has not been previously recognized. In Table 1, only $p = 8/9$ was considered. In Figure 7, p is variously set at $1/9, 2/9, \dots, 8/9$. Similar distributions could be determined empirically (or possibly using the Gamma function generalization of the factorials in the binomial coefficient) for any real p , but the binomial distribution gives the probabilities for integer N and hence, only for p where pb^E is integer.

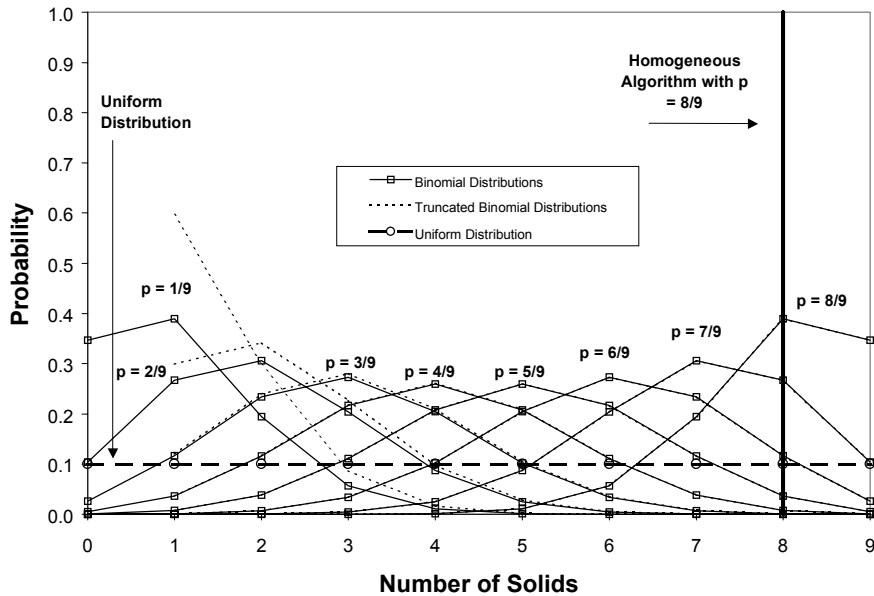


Figure 7. Binomial, truncated binomial, uniform, and Dirac distributions of the number of solids as a function of p .

These distributions are discrete and are shown as curves only for clarity. A Dirac Delta distribution ($P = \delta(8-N)$), corresponding to the homogeneous algorithm for $p = 8/9$) and a discrete uniform distribution ($P = 1/10$ for all N) are also shown for comparative purposes. Each p value has a similar Dirac Delta distribution when the homogeneous algorithm is applied. The labeled curves give the distributions of N for different values of p . These distributions are generally asymmetric and non-normal. The decision to retain individual squares in the construction of the fractal is based on independent Bernoulli trials. The problem is the same as asking "What is the probability of obtaining N heads in b^E flips of an unbalanced coin?" We set the degree of imbalance as the cutoff p ; that is, we decide that if a random number in $[0,1]$ is greater than p , we have a 'head'. The probability of each possible outcome ($N = 0, 1, \dots, b^E$) can be computed directly from the binomial distribution. Following Freund [1971], we have

$$B(N) = \binom{b^E}{N} p^N (1-p)^{b^E-N} \quad (7)$$

where $B(N)$ is the probability of N successes in b^E trials and $\binom{b^E}{N}$ is the binomial coefficient.

The use of the analytical form of these distributions allows computation of the exact probabilities of relatively infrequent conditions that cannot be readily determined from a sample of realizations. Indeed, focusing on the $p = 8/9$ case for example, the instances of 3, 2, 1, or 0 solids have probabilities of 1.1×10^{-4} , 5.9×10^{-6} , 1.8×10^{-7} , and 2.6×10^{-9} respectively. This attests to the near-impossibility of relying on multiple realizations to completely describe the variability of prefractal structures generated with the heterogeneous algorithm; more than 1 billion realizations would be required.

The asymmetry has important effects on the porosity. For example, the probability density curve for $p = 8/9$ has a mean value equal to the desired value of 8 solids. Nevertheless, the asymmetry in the distribution means that the case in which there are 9 solids will be realized much more frequently than the case in which there are 7 solids. Therefore, it is likely that the porosity this type of prefractal 'inherits' from its first iteration will be smaller than the expected value. Figure 5 is an example. When 3 or more random values fall above $8/9$ (>5% probability) there will be 6 (or fewer) solids and a porosity much larger the expected porosity will result. Clearly, a significant number of realizations have to be averaged to provide a mean porosity within close tolerance of its true value. This is essentially the case when many 'fractal patches' or fractal cell arrays are assembled into a single porous structure as done in some of the simulations of Bird and Dexter [1997] and Rappoldt and Crawford [1999]. This method also imposes an upper bound smaller than the size of the domain on the fractal scaling.

As examples of the impact of the heterogeneous algorithm on porosities, we consider some simple 2-dimensional porous media. The actual porosity ϕ in terms of the solid probability (p) at any iteration level and the iteration level (i) for prefractals generated using the homogeneous algorithm is always given by Equation (5). For example, for the homogeneous $b = 3$, $i = 4$, $p = 8/9$ porous structures in Figure 1 and Figure 4, Equation (5) gives $\phi = 0.376$. In contrast, the actual porosity of the structure in Figure 5, which has the same parameters but was generated with the heterogeneous algorithm, is 0.151. This value differs appreciably from the porosity computed with Equation (5). An equation

similar to Equation (3) can be developed to express the porosity of structures generated with the heterogeneous algorithm but it must keep track of what effective p is realized at each of the $b^{E(i-1)}$ sites for each iteration i , and quickly becomes unmanageably cumbersome. Moreover, the dependence of the porosity on the sequence of p realized means that it is not possible to have a general predictive expression other than perhaps one that makes broad probabilistic statements.

Figure 8 compares the distributions of porosity observed for 1000 structure realizations generated with the heterogeneous algorithm to the same distributions for the homogeneous algorithm (actually the homogeneous results have only one value each).

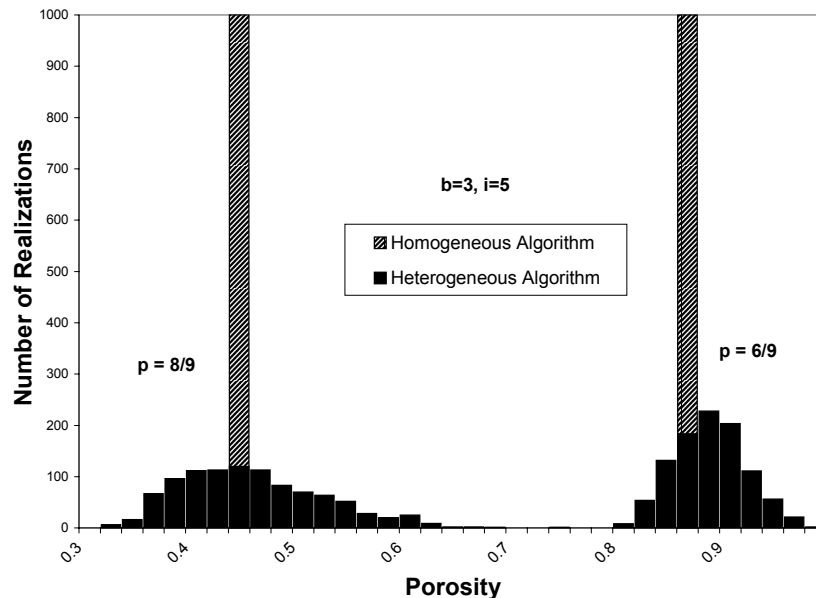


Figure 8. Distributions of porosity for 1000 realizations of homogeneous and heterogeneous algorithms at $p = 8/9$ and $p = 6/9$ with $b = 3, i = 5$.

Theoretically, the distributions of ϕ from the heterogeneous algorithm must cover the entire range of possible porosities ($0 \leq \phi \leq 1$) because, as pointed out earlier, there is a finite probability of, for example, 0 solids when $p = 8/9$, or similarly, of 9 solids when $p = 1/9$. Clearly, the sample of 1000 realizations considered in Figure 8 does not explore the entire range.

For larger values of the fractal scaling parameter b , the magnitude of the porosity deviations that arise from the heterogeneous algorithm will be reduced. However, the range in b values that might be most applicable to soils remains an open question [Brakensiek and Rawls, 1992; Tyler and Wheatcraft, 1992; see also Chapter 2].

Our ultimate concern is with the computationally intensive fluid and transport simulations in fractal porous media. It is not realistic that such simulations can be carried out on a statistically representative number of generated media. Using the homogeneous algorithm to generate the media completely eliminates the variability in total porosity and implies that results that can be meaningfully related to the fractal parameters can be obtained from fewer realizations. In one sense, we are comparing zero variability with potentially large variability that is a complex function of the fractal generating parameters.

Much of the work of others that uses the heterogeneous algorithm does not involve multiple realizations, despite the great potential range in porosities. If a modeler were particularly unlucky, the porous medium would entirely disappear. This forces those who use such models to make subjective choices about which realizations are 'acceptable'. For example, neither Rapoldt and Crawford [1999] or Bird and Dexter [1997] would have computed diffusion or water retention in pure void spaces had these possible structures been generated.

One way to avoid this difficulty is to constrain the possible values of N to exclude 0. This eliminates two other problems that arise when $N = 0$. First, $D = \log(0)/\log(b)$ is undefined. Second, the term $(N/b^E)^{-q}$, which is needed for the multifractal computations below, is undefined for any positive q . This constraint on the binomial distribution has appeared in other contexts as the truncated binomial distribution [Patil, 1962]. The formula for the computation of the truncated binomial distribution is

$$B_t(N) = \frac{\binom{b^E}{N} p^N (1-p)^{b^E-N}}{\sum_{N=1}^{b^E} \binom{b^E}{N} p^N (1-p)^{b^E-N}} \quad (8)$$

The summation in the denominator excludes $N = 0$ and normalizes the probability density to 1. This distribution is also shown on Figure 7. The deviation from the binomial distribution is large for $p = 1/9$. The difference between the distributions gets smaller as p increases and is insignificant at $p = 4/9$. The multifractal considerations below use the truncated binomial distributions. Despite the simplicity of the required modifications, no implementations of the heterogeneous algorithm that use this approach are known to exist, other than the codes presented in Appendices A and B.

A related issue is that, for relatively small values of b and i , probabilities that can actually be realized at low iteration levels are strongly discretized. For example, in the 2-dimensional, $b=3$ Sierpiński carpet prefractals presented by Bird and Dexter [1997], the actual proportions of solid blocks that can be converted to pores at the first iteration level is limited to the following ten possibilities: $0/9$, $1/9$, $2/9$, $3/9$, $4/9$, $5/9$, $6/9$, $7/9$, $8/9$, or $9/9$. Note that $p_{\text{pore}} (= 1 - p) = 0.1$ as used in Bird and Dexter [1997], which, while close to $1/9 (= 0.111\dots)$ cannot actually be realized during the early construction stages of this prefractal.

Models generated with the heterogeneous algorithm represent a particular case of models that can be classified as heterogeneous [Gouyet, 1996] as opposed to the homogeneous model we present in Figure 4. The defining characteristic of a heterogeneous model is that the mass ratio $\beta = N/b^E$ (the effective p) varies. Mandelbrot [1983] calls this method 'canonical curdling'. For use as models of porous media as implemented here, heterogeneous fractals have the undesirable feature of uncontrolled porosity. The distribution of the β can be explicitly defined for the construction of heterogeneous fractals [Gouyet, 1996]. The heterogeneous algorithm as considered here however results in heterogeneous fractals for which the distribution of β depends on the value of p in a complex way (Figure 7) that has not been recognized in previous literature.

Heterogeneous fractals have a multifractal nature [Gouyet, 1996]. This means that they no longer possess global scale-invariance and instead of being well characterized by a single fractal dimension, require a spectrum of dimensions for their description. Saucier and Muller [1993] applied multifractal methods to porous media but, unlike the methods we focus on here, treated the porosity as a measure on a Euclidian support. Following the approach of Benzi et al. [1984] and Paladin and Vulpiani [1987], who used a random β model for energy transfer in turbulent flows, the multifractal spectra for the heterogeneous algorithm are computed based on the probability distributions, $P(\beta)$, in Figure 7.

First we define the average $\{f(\beta)\}$ (where f is an arbitrary function of β) of the probability distribution as

$$\{f(\beta)\} \equiv \int P(\beta) f(\beta) d\beta \quad (9)$$

A set of exponents $\Phi(q)$ can be defined by a generalization of $N = r^{-D}$ as follows:

$$\lim_{r \rightarrow 0} \langle n(r)^q \rangle \propto r^{\Phi(q)} \quad (10)$$

where $n(r)$ is a local density, q is an index, and $\langle \rangle$ denotes a spatial average. The $\Phi(q)$ are computed as

$$\Phi(q) = Eq - \log_b \{ \beta^{-q} \} \quad (11)$$

where Equation (9) is used with $f(\beta) = \beta^{-q}$. Because $P(\beta)$ is discrete in this case, the integral in (9) is simply a summation of the form $P(\beta_1)\beta_1^{-q} + P(\beta_2)\beta_2^{-q} + \dots$

The $\Phi(q)$ can be converted to generalized or Renyi dimensions according to $D_{q+1} = \Phi(q)/q$ [Paladin and Vulpiani, 1987]. Next, the D_q can be converted to $\tau(q)$ with $\tau(q) = (1-q)D_q$, and finally, α and $f(\alpha)$ can be calculated from $\tau(q)$ via [Gouyet, 1996]

$$\alpha(q) = -\frac{d}{dq}\tau(q) \quad (12)$$

and

$$f(\alpha(q)) = \tau(q) + q\alpha(q) \quad (13)$$

Equations (12) and (13) form the basis of the typical multifractal spectrum.

The use of these equations for the calculation of the multifractal spectra is illustrated in detail for one example below. The following Tables give the probabilities and the calculations for $p = 8/9$. Table 2 lists the binomial probability values of different $\beta = N/b^E$. For $p = 8/9$, the difference between the binomial and truncated binomial distributions is on the order of one part in 10^9 .

Table 2. Binomial Probabilities for $p = 8/9$. These are effectively equivalent to the truncated binomial probabilities for this p value.

β	$P(\beta)$
1	0.346439
0.888889	0.389744
0.777778	0.194872
0.666667	0.056838
0.555556	0.010657
0.444444	0.001332
0.333333	0.000111
0.222222	5.95E-06
0.111111	1.86E-07
0	2.58E-09

Table 3 illustrates the computation of the multifractal spectrum. q values are selected arbitrarily, though it is important that the asymptotic limits (where α and $f(\alpha)$ cease to change significantly) are reached. The example calculation here uses integer q in the range $-10 \leq q \leq 10$, but the spectra presented below use $-50 \leq q \leq 50$. Only 3 significant figures are included in the table values. $\Phi(q)$ were computed from (9) using the summation $P(\beta_1)\beta_1^{-q} + P(\beta_2)\beta_2^{-q} + \dots + P(\beta_{10})\beta_{10}^{-q}$ where the $P(\beta_i)$ are the exact probabilities (Table 2) from the binomial distribution, and the β_i are the possible ratios of retained sites to total sites each time such a selection is made (i.e., $1/9, 2/9, \dots, 9/9$). Given that the $P(\beta_i)$ are truly discrete in the problem at hand, the summation is the proper way (and perhaps the only way) to compute the integral in (9).

Table 3. Computation of Multifractal Spectrum for $p = 8/9$.

q	$\Phi(q)$	D_q	$\tau(q)$	$\alpha(q)$	$f(\alpha)$
-10	-19.3				
-9	-17.4	1.93	19.3		
-8	-15.4	1.93	17.4	1.96	1.69
-7	-13.5	1.93	15.4	1.96	1.72
-6	-11.5	1.92	13.5	1.95	1.76
-5	-9.57	1.92	11.5	1.94	1.79
-4	-7.64	1.91	9.57	1.94	1.82
-3	-5.71	1.91	7.64	1.93	1.85
-2	-3.80	1.90	5.71	1.92	1.87
-1	-1.89	1.90	3.80	1.91	1.89
0	0.00	1.89	1.89	1.90	1.89
1	1.88		0.00	1.89	1.89
2	3.74	1.88	-1.88	1.87	1.86
3	5.58	1.87	-3.74	1.85	1.81
4	7.39	1.86	-5.58	1.83	1.73
5	9.17	1.85	-7.39	1.79	1.58
6	10.9	1.83	-9.17	1.74	1.29
7	12.4	1.81	-10.9	1.62	0.47
8	13.5	1.77	-12.4	1.30	-2.03
9	13.9	1.68	-13.5	0.76	-6.67
10	14.0	1.55	-13.9		

Next, the $\Phi(q)$ were converted to generalized dimensions according to $D_{q+1} = \Phi(q)/q$ [Paladin and Vulpiani, 1987]. Then, the D_q were converted to $\tau(q)$ with $\tau(q) = (1-q)D_q$. These conversions imply $\tau(q) = -\Phi(q-1)$ and this equivalence is clear in Table 3. Here however the notation has been retained in its original form to maintain close correspondence with the cited works that will enable interested readers to follow the application of the equations.

The α were calculated from $\tau(q)$ via Equation (12). This was carried out as a centered finite difference (i.e., $\alpha = [\tau(q+1) - \tau(q-1)]/2$; see Table 3).

Finally, $f(\alpha)$ were calculated with Equation (13).

Figure 9 shows the multifractal spectra for 8 of the possible p values ($p = 1/9, p = 2/9, \dots, p = 8/9$) when the truncated distributions of the number of solids that arise from the heterogeneous algorithm (Figure 7) are taken into account. The peaks of these spectra correspond to the fractal dimension of the self-similar fractals that would be generated with the homogeneous algorithm, except that the use of the truncated distributions causes deviations at small p . Hence, the peaks decrease systematically from $f(\alpha) = 1.89\dots$ for $p = 8/9$ to $f(\alpha) \approx 0.63\dots$ for $p = 2/9$. The peak for the truncated $p = 1/9$ case is $0.38\dots$ instead of the $D = 0$ that applies to the homogeneous case. The spectra for homogeneous fractals collapse to single points that correspond approximately to the peaks of the $f(\alpha)$ curves. Thus, the single Dirac spike representing the probability distribution for the homogeneous algorithm with $p = 8/9$ (Figure 7), corresponds to a single point at $f(\alpha) = 1.89\dots$ on the $p = 8/9$ spectrum. In contrast, the horizontal line corresponding to the truncated uniform distribution on Figure 7 (which has a mean of $N = 5$) translates to a broad multifractal spectrum with a peak at $D = \log(5)/\log(3) = 1.465\dots$

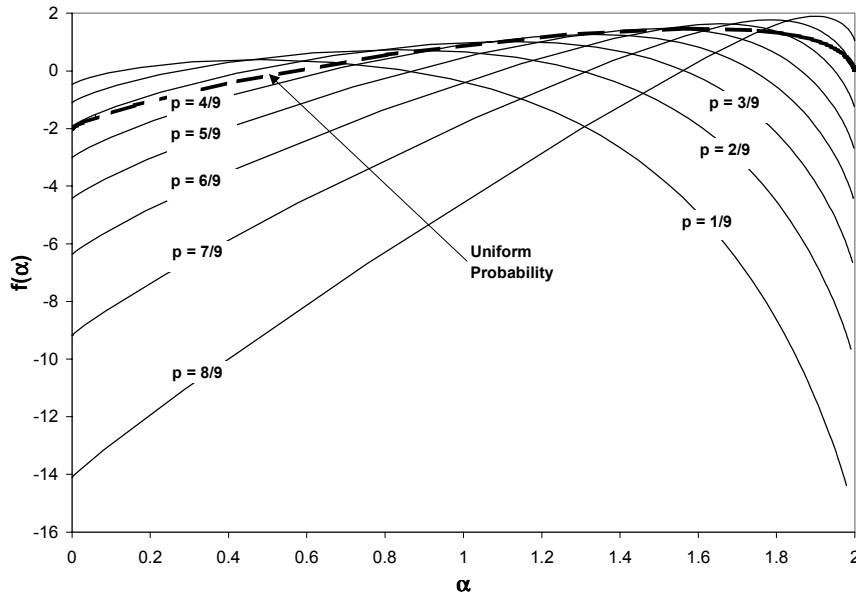


Figure 9. Multifractal spectra for 2-dimensional Sierpiński carpets with $p = 1/9, 2/9, \dots, 8/9$. Spectrum for uniform distribution also shown.

The $f(\alpha)$ need not be positive according to Evertsz and Mandelbrot [1992], Mandelbrot [1990], and Mandelbrot [1991]. In fact, negative $f(\alpha)$ contain important information on the sampling variability [Mandelbrot, 1990].

All of the complexity associated with the multifractal approach arises only as a result of the heterogeneous algorithm. The models generated using the heterogeneous algorithm are not necessarily improper models of porous media; However, there is a potential discrepancy between porous structures generated in this way and simple fractal scaling laws and porosity computations. To control variability in porosity and pore size distributions in different realizations and in work by different scientists, it would seem that the homogeneous algorithm, which honors simple fractal scaling and has predictable porosity, should be preferred over the heterogeneous algorithm.

1.4 Computer Codes

To make models of prefractal 2- and 3-dimensional porous media more widely available to interested researchers, two MATLAB® codes are provided in Appendices A and B.

Non-random, random homogeneous, and both binomial and truncated binomial random heterogeneous algorithms have been implemented. These codes offer rudimentary graphics and provide ASCII output of the prefractional media for use in other applications or graphics packages. The 2-dimensional output is available in bmp or GRIDASCII format, or as lines containing triplets of x, y, and 0 or 1 corresponding to the absence or presence of a solid respectively. The third option is much slower and memory intensive. The 3-dimensional ASCII output is in the form of x, y, z, and 0 or 1. Complete listings are provided in the Appendices and the codes are also available in electronic form from the author. Figure 6 shows examples of the graphical output from the 3-dimensional code. The fractal generating parameters are $b = 3$, $i = 3$, and $D = 2.72\dots$ (a randomized variant of the standard Menger sponge). Such models should prove useful for generation of random 2- and 3-dimensional porous media in which the retention and transport of fluids, solutes, particles, and organisms can be simulated.

1.5 Conclusions

The heterogeneous algorithm that has been used to generate prefractional models of porous media in a number of soil investigations leads to a type of multifractal structure that has several drawbacks. In particular, for smaller values of the b scaling factor, the porosity can vary widely from the expected value in individual realizations. This algorithmic artifact is eliminated with the homogeneous algorithm. Porosity variations are likely to affect most processes of interest in structures generated with the heterogeneous algorithm. The increased variability in computed soil water retention that results from application of the heterogeneous algorithm, as compared to results obtained with the homogeneous algorithm, is demonstrated in Chapter 3.

Prefractional models offer a convenient means of generating complex porous media in a rigorous and reproducible manner. More applications to water retention and flow, fragmentation studies, soil biota, and gas/solute transport are expected. Computer codes for the homogeneous and binomial and truncated binomial algorithms are provided as a means for researchers to more easily create and experiment with prefractional porous media.

Chapter 2. Percolation Thresholds in 2-Dimensional Prefractal Models of Porous Media

2.0 Summary

Considerable effort has been directed towards the application of percolation theory and fractal modeling to porous media. Here, these research areas are combined to investigate percolation in prefractal porous media. Percolation thresholds are estimated for the pore space of homogeneous random 2-dimensional prefractals as a function of the fractal scale invariance ratio b and iteration level i . The percolation thresholds for these simulations increased beyond the 0.5927... porosity expected in Bernoulli (uncorrelated) percolation networks. Percolation in prefractals occurs through large pores connected by small pores. The thresholds increase with both b (a finite size effect) and i . The results allow the onset of percolation in models of prefractal porous media to be predicted and can be used to bound modeling efforts. More fundamental applications are also possible. Only a limited range of parameters has been explored empirically but extrapolations allow the critical fractal dimension for a large combination of b and i values to be estimated. Extrapolation to infinite iterations suggests that there may be a critical fractal dimension of the solid at which the pore space percolates. The extrapolated value is close to 1.89 -- the well-known fractal dimension of percolation clusters in 2-dimensional Bernoulli networks.

2.1 Introduction

2.1.1 Percolation

Percolation is an important research area in physics (e.g., Stanley et al., 1999; Stauffer and Aharony, 1992; Bunde and Havlin, 1996). Applications of this research are exceedingly broad and range from modeling forest fires to predicting human social phenomena [Solomon et al., 2000]. Berkowitz and Balberg [1993] and Berkowitz and Ewing [1998] have reviewed applications in groundwater hydrology and soil physics. Sahimi [1994] has discussed many other applications. A primary motivation for studying

percolation in porous media is the desire to predict macroscopic connectivity across the pore network. Transport can only occur in a connected medium. A benefit of studying percolation is that the first level of the complexity of the connected pore network is quantitatively elucidated. Basically, we can determine the onset of sample-spanning connectivity and the statistical form of the connected network quantitatively, even when the structure of the porous medium is completely disordered.

Our focus here is on one of the simplest 2-dimensional percolation models -- site percolation -- and its application in fractal porous media. Site percolation can be described quite simply: on a lattice randomly populated with pores and solids, occupied or unoccupied lattices sites (squares in 2 dimensions) are considered connected if they share an edge. We refer to such a lattice as Bernoullian; its distribution of pores and solids lacks any spatial correlation. Percolation across the lattice occurs when a connected path exists from one side of the lattice to an opposite side. The upper right portion of Figure 10 illustrates the concept. Solids are shown in black, pores unconnected to the top boundary in white, and pores along the top boundary in red or gray. The connected percolation cluster is shown in red. Despite the small size of this lattice, the complex morphology of the percolating cluster -- including a convoluted boundary and 'holes' of various sizes inside the cluster -- is apparent.

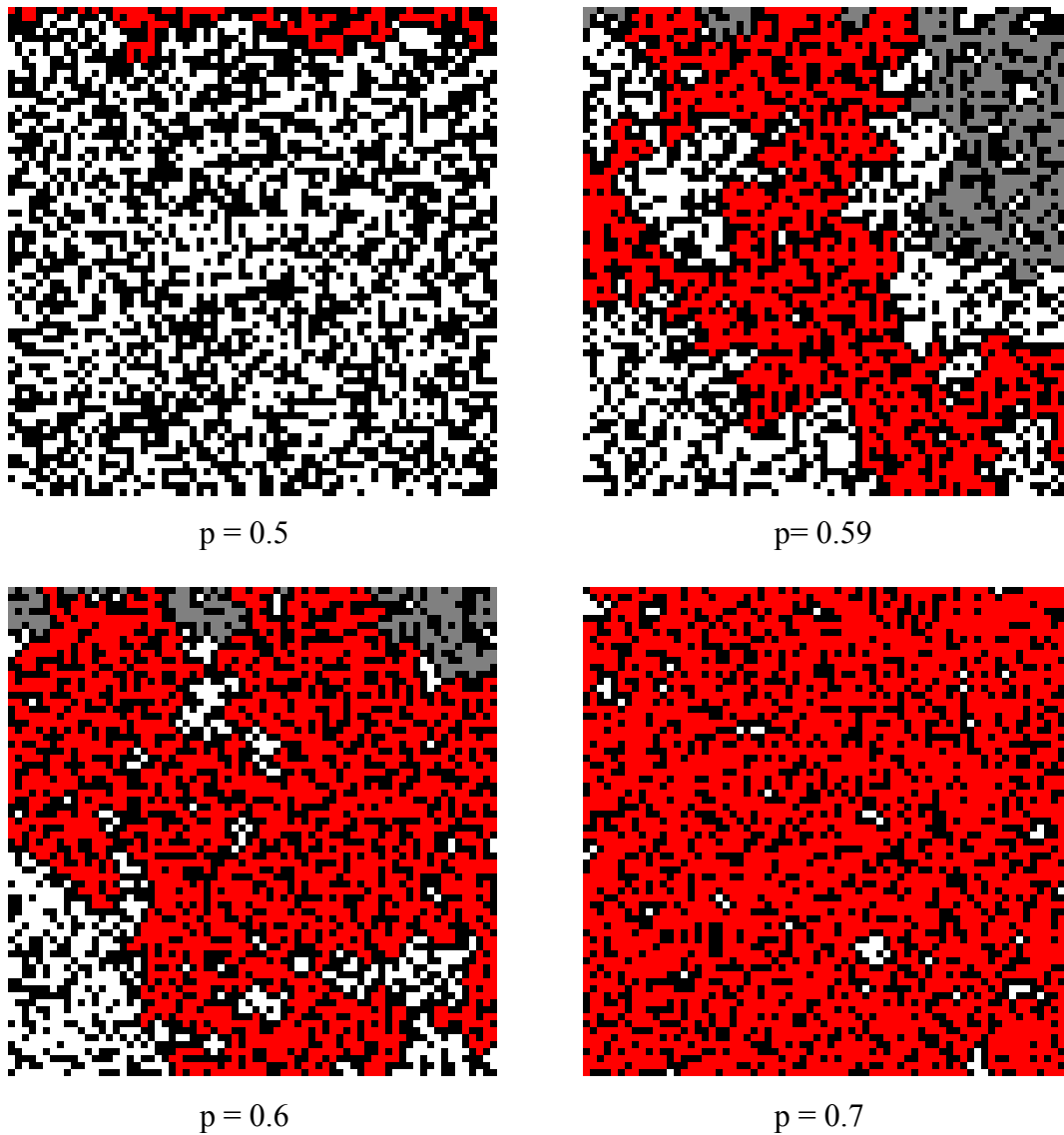


Figure 10. Connectivity to top boundary as a function of pore probability. Solids black, pores unconnected to top boundary white, pores connected to top boundary red or gray.

One of the remarkable discoveries in such simple models is the existence of a persistent and, when the lattice is large enough, sharp 'percolation threshold'. For site percolation in a 2-dimensional Bernoullian lattice, this threshold is reached at a conducting site concentration of 0.5927.... This value, known as the critical concentration p_c , has been determined empirically and has thus far eluded theoretical efforts to compute it, although

renormalization methods (e.g., Perreau et al, 1996; see below) come close. When the probability p of a conducting site (in our case a pore) is less than p_c , percolation is highly unlikely, and, when p is greater than p_c , percolation is nearly certain. The probabilistic notions of 'highly unlikely' and 'nearly certain' depend primarily on the lattice size. For increasing lattice size, the cumulative probability distribution of percolation frequency for multiple random lattice realizations approaches a Heavyside function.

Figure 10 shows how site connectivity to the top boundary changes with increasing pore probability p for a 70×70 lattice and illustrates the onset of percolation through the lattice near p_c . At $p < p_c$, all pores that connect to the top boundary (red) are effectively isolated from the interior of the network and percolation does not occur. Increasing the porosity to $p \approx p_c$ causes the network to percolate from top to bottom. Further increases in porosity cause more of the pore space to be connected.

Obviously, the pore probability is equivalent to the porosity. That the 2-dimensional value of p_c is greater than the porosity of many porous media that are known to be permeable (i.e., to percolate) points out one important limitation of these 2-dimensional models. The percolation threshold for site percolation in 3 dimensions -- where the sites are elementary cubes and connectivity occurs when a face is shared -- is 0.3116... [Stauffer and Aharony, 1992].

Of course, there are other significant limitations to the application of such simple models to real soils and aquifer or reservoir materials. There is no anisotropy or inhomogeneity and no secondary porosity. There is also no potential for film connectivity that may dominate soils and other un- or weakly-consolidated media.

On the other hand, percolation models present highly tortuous paths and a significant 'dead-end' pore system. This morphology can be quantified by another remarkable property of Bernoullian percolation lattices: the percolating cluster always has a particular fractal dimension.

Chapter 1 contains a brief introduction to fractal geometry. Randomization of porous fractal models consists of simply distributing the N remaining solids at each application of the fractal algorithm randomly about the b^E sites in the sublattice being created. In this Chapter, we use a fixed value of N (corresponding to a homogeneous fractal). Sometimes N is varied according to probabilistic rules, leading to a heterogeneous fractal with uncontrolled porosity [Sukop et al., 2001a].

There has been a preference for the use of heterogeneous fractal algorithms to construct porous media [Chayes, 1995; Raploft and Crawford, 1999; Bird and Dexter, 1997]. Mandelbrot [1983] recommended the heterogeneous algorithm as simpler to program and to treat analytically than the homogeneous algorithm. In contrast, Chayes [1995] suggested that homogeneous fractals were much easier to analyze. A serious limitation of the heterogeneous approach for modeling porous media is that the porosity of a given realization cannot be predicted. All of the percolation measurements here are conducted on homogeneous fractals. The homogeneous approach also avoids the complication in which the fractal 'disappears' when the realized value of N is 0 at the first iteration.

This work is limited to fractals that exist in 2-dimensional space. It is expected however, that the results can be readily generalized to 3-dimensional space as most other phenomena related to fractal scaling can. Such generalization is only qualitative at this time. Direct computation of the 3-dimensional results will be possible as improved algorithms and greater computational power become available.

2.1.3 Sierpiński Carpet as Percolation Cluster Model

The number of elements N in a 2-dimensional percolating cluster near p_c varies with the number of elements n in the array as $N \sim n^{91/96}$ [Turcotte, 1992]. The basic fractal scaling law $N = b^{iD}$ has the same form. For a lattice with b^i sites on its edge, the number of elements n in the array equals b^{2i} . Thus, $N \sim b^{2i \cdot 91/96} = b^{iD}$. This implies that $D = 2 \times 91/96$ or $D = 1.895\dots$. This is very close to the fractal dimension of the Sierpiński carpet: $D = \log 8 / \log 3 = 1.892\dots$, which suggests that the Sierpiński carpet is a reasonable

model of a Bernoullian percolation cluster. Figure 11 shows a comparison between a percolation cluster and a randomized Sierpiński carpet.

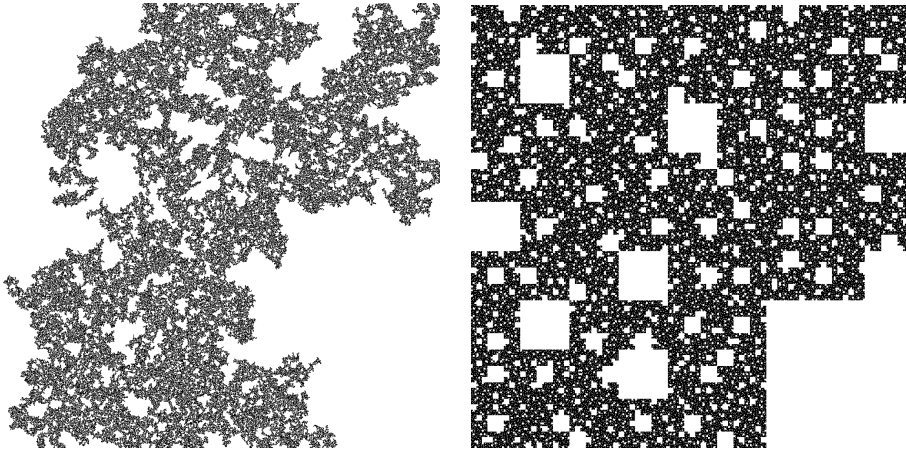


Figure 11. Comparison between percolation cluster in Bernoullian lattice (1024 x 1024) at p_c with randomized Sierpiński carpet ($b = 3$, $N = 8$, $i = 6$). Percolation cluster measured $D = 1.839\dots$, Randomized carpet $D = 1.892\dots$

The qualitative similarities between these images are significant. First, both have complex boundaries. Second, both the cluster and the carpet have 'holes' with a broad range of sizes. More importantly, there is a quantitative agreement between the two structures that has led to significant interest in fractals among the physics community involved in research on disordered systems.

Similar results for the percolation threshold and fractal dimension are available for three-dimensional lattices. The site percolation threshold is 0.3117 and the fractal dimension of the percolating cluster is $D = 2.524\dots$ [Bunde and Havlin, 1996].

Fractals are popular as models of percolation phenomena in solid materials (electrical conduction for example) because of these observations. The percolation thresholds and the critical behavior of fractals have been investigated in the physics literature [Geffen et al, 1983; Geffen et al, 1984a,b; Yu and Yao, 1988a,b; Machta, 1991; Perreau et al., 1996; Lin and Yang, 1997].

2.1.4 Another perspective: Fractal Porous Media

The viewpoint adopted in the presentation of percolation in a random medium as discussed above rather naturally suggests a physical model -- perhaps a homogeneous sandstone -- into which a fluid might move along connected paths and lead to fractal patterns similar to those shown in Figure 11.

However, probably as a result of observed power law behavior of moisture retention curves of natural porous media [Brooks and Corey, 1964; Campbell, 1985; see also Chapter 3], significant effort has been expended on a much different approach in the application of fractals to porous media [Ahl and Niemeyer, 1989; Tyler and Wheatcraft, 1990; Adler and Thovert, 1993; Crawford and Matsui, 1996; Bird and Dexter, 1997; Perfect, 1999]. The porous medium itself is assumed to follow a fractal model in this approach. To a lesser extent, the pore space has been considered to follow fractal scaling by some authors.

Exploring the fractal solid approach, we consider randomized Sierpiński carpets as models of physical structures, in which the solids are represented by the fractal set and the voids are represented by that set's complement. Crawford and Matsui [1996] have found that 'mass fractals' like those we consider here are likely to be most relevant to natural porous media, despite discussion in the soils literature regarding 'pore fractals' [Rieu and Perrier, 1998]. The apparent inability of either type of fractal model to simulate porous materials that simultaneously have broad ranges of pore sizes and solid particle sizes may limit their generality. 'Pore-solid fractals' [Bird et al., 2000] have been introduced as more general models to address this issue. This is one of the critical questions for the application of fractal models to natural porous materials but it is not considered further here. Adler and Thovert [1993] have reviewed the construction and transport properties of exactly self-similar deterministic fractal porous media while Dullien [1991] has reviewed the pore-level characterization of porous media.

The porosity (ϕ) of a 'true' fractal (in which the generating process is iterated an infinite number of times) is always unity. Hence, such models are of little use as models of

natural porous media such as soil, aquifer, or reservoir material. However, by introducing a lower 'cutoff' size, where the generating process ceases, we can maintain a realistic porosity. Thus, we can define such a 'prefractal' [Feder, 1988] in terms of any three of the following four parameters: D , b , i , and ϕ (or equivalently p or N). Equation (2) expresses the relationship between these parameters in terms of the total porosity for a prefractal embedded in E -dimensional space.

Rappoldt and Crawford [1999], and Bird and Dexter [1997] have presented a simple method of introducing an upper cutoff, beyond which fractal scaling does not apply and the medium becomes statistically translation-invariant (rather than scale-invariant), by assembling fractal 'patches' into a larger porous medium. The results obtained here can provide bounds for percolation in such media.

2.1.5 Use of Fractal Dimension for Bernoulli Percolation

Usually we reserve the terms fractal or prefractal for structures that exhibit fractal scaling over multiple scales (iteration levels). Thus, it initially seems improper to utilize the fractal dimension D as a surrogate for porosity and the fractal scale invariance ratio b for a lattice size parameter in the Bernoulli case. Nevertheless, we find that these quantities from the general fractal case extend to the Bernoulli or first iteration case without difficulty. At the very least, this extension saves us from having to treat the first iteration case separately.

2.2 Literature Review

There are three principal research areas that pertain to our problem. We consider two of these below. The third area is mathematical research that appears in a handful of papers [Chayes, et al., 1988; Chayes and Chayes, 1989; Chayes, 1995]. These papers illustrate the difficulty of an analytical approach to this problem.

2.2.1 Percolation in Correlated Systems

For more than one fractal iteration, fractal media clearly exhibit spatial correlation because large holes can be considered as a group of coalesced small holes. At the first

fractal iteration level however, these media are identical with standard percolation lattices. A number of studies examine percolation in spatially correlated systems.

Mani and Mohanty [1999] summarized the work of five researchers and concluded that: "Bond and site percolation thresholds generally decrease in the presence of finite-range spatial correlation." Odagaki et al. [1999] used a unique method to impose correlation in which the number of nearest neighbors in a conducting cluster served as a correlation length. Overall, the percolation thresholds were observed to increase as the spatial correlation increased. These results conflict with those reported by Mani and Mohanty [1999]. A much earlier paper by Duckers and Ross [1974], and subsequent work by Duckers [1978] may resolve this conflict. These papers show, for 2- and 3-dimensional systems respectively, that increasing the strength of the correlation first decreases and then increases the percolation threshold.

Nauman [1993] presented an algorithm for generating correlated media with a given conditional probability that an occupied site (pore or solid) is adjacent to another occupied site and used it to develop phase diagrams for percolation in 2 and 3 dimensions.

2.2.2 Percolation on Fractals

Yu and Yao [1988a] investigated site percolation on triangular Sierpiński gasket networks. From simulations with random site occupations, they found that the percolation threshold increased as the number of fractal iterations increased such that $p_c = 1 - 1/i$. By extrapolation, this leads to $p_c = 1$ for infinite iterations. In a subsequent study, Yu and Yao [1988b] considered a random occupation of sites on the fractal set parts of deterministic Sierpiński carpets of extreme lacunarity. As the fractal dimension of the starting set decreased, the percolation thresholds increased. This work is essentially a network simulation rather than a model of a physical structure in the sense that we apply randomized carpets here.

In a very similar study, Lin and Yang [1997] considered site percolation on Sierpiński carpets of differing lacunarity. Figure 12 illustrates their approach to the percolation problem. Sites in the solid phase are randomly assigned either conductive or insulating properties according to the site occupation probability p being evaluated. The pores are always insulating obstacles. The conclusions of this study are the same as those of Yu and Yao [1988b]. The fixed positions of the pores and the focus on percolation in the solid phase in this view of a percolating system cause it to have limited relevance for the randomized carpet porous media systems of primary interest to us.

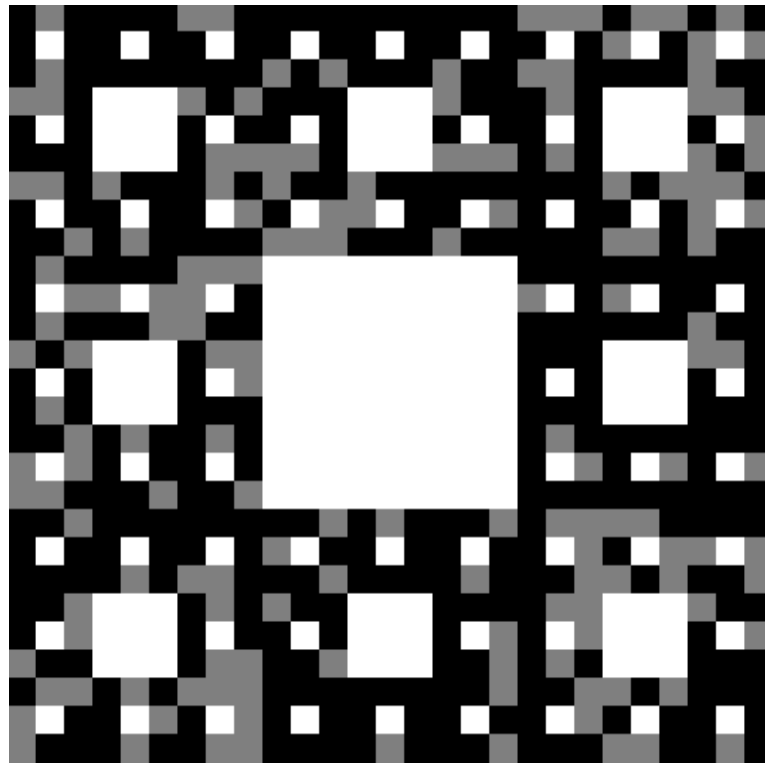


Figure 12. Lin and Yang [1997] approach to percolation on fractal set problem. Conducting solids black, non-conducting solids gray, and pores white.

Perreau et al. [1996] used renormalization to investigate percolation of the fractal set part (the solids) of homogeneous randomized Sierpiński carpets. These results are discussed in detail below.

2.3 Methodology

2.3.1 Hoshen-Kopelman Algorithm

We use the Hoshen-Kopelman algorithm [Stauffer and Aharony, 1994; Bunde and Havlin, 1996] to determine connectivity of the lattice pore sites. All clusters are uniquely identified. The algorithm is demonstrated on a 5×5 lattice in Figure 13. The algorithm begins with the assignment of temporary labels to void sites at the upper left corner and ends at the lower right corner (Figure 13, center). The first void site is labeled 1 and the neighboring site gets the same label because it is connected to the same cluster. The third site is a solid and the fourth is labeled 2 because it is unknown if it is connected to cluster 1. In the second row, the first site is connected to its neighbor at the top and is therefore labeled 1. The next void site does not have a neighbor void site at the top or left and is labeled 3. The next site is now the neighbor of sites labeled 2 and 3. All three sites belong to the same cluster. In this situation, the site gets the label of the left site, which is 3. The label 2 from the site above is put in an array to keep track that clusters 2 and 3 are connected. This method is continued until all the void sites in the lattice are labeled.

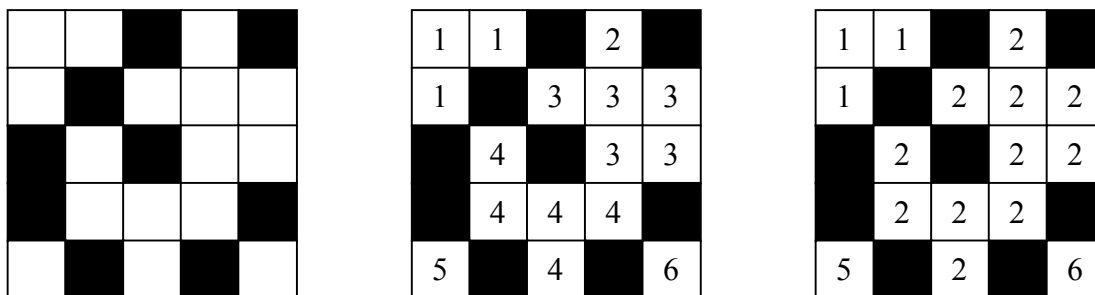


Figure 13. Hoshen-Kopelman algorithm.

The final step of the Hoshen-Kopelman algorithm is to change the initial labels into the final ones that represent the individual clusters (Figure 13, right). A single cluster that connects two opposite sides of the lattice (e.g., cluster 2 in Figure 13) is a 'sample-spanning cluster' or simply a percolation cluster.

2.3.2 Determination of Percolation Thresholds in Prefractals

The percolation thresholds 0.5927 and 0.3111 for 2- and 3-dimensional site percolation discussed above are values of p_c at which an infinite cluster appears in an infinite network. Out of necessity, we work with finite lattices. In finite systems the percolation thresholds are not as sharply defined, which means that there are non-zero probabilities of finding percolation at concentrations of void sites lower than p_c and of finding failure to percolate at concentrations higher than p_c .

Under these conditions, the percolation threshold can be defined as the porosity where the chance of percolation is 50%. The porosity of the network (the pore space of the fractal) depends on three fractal parameters according to Equation (2). The thresholds are determined for lattices with the same scale invariance ratio. To realize different porosities in the lattice, the iteration level or the probability is changed.

To determine the percolation thresholds, 100 realizations of prefactal structures corresponding to a particular set of fractal parameters were constructed. Each structure was checked for horizontal and vertical percolation using the Hoshen-Koppelman algorithm. The empirical frequency of percolation is taken as an estimate of the probability of percolation and corresponds to a single point in a graph such as Figure 14. Incrementing the fractal generating parameters leads to a different porosity and a new point. The percolation threshold is then determined by fitting the cumulative normal distribution function to the estimated points with a least-squares method as done by Lin and Yang [1997]. The mean represents the threshold and the standard deviation gives an indication of the sharpness of the distribution function.

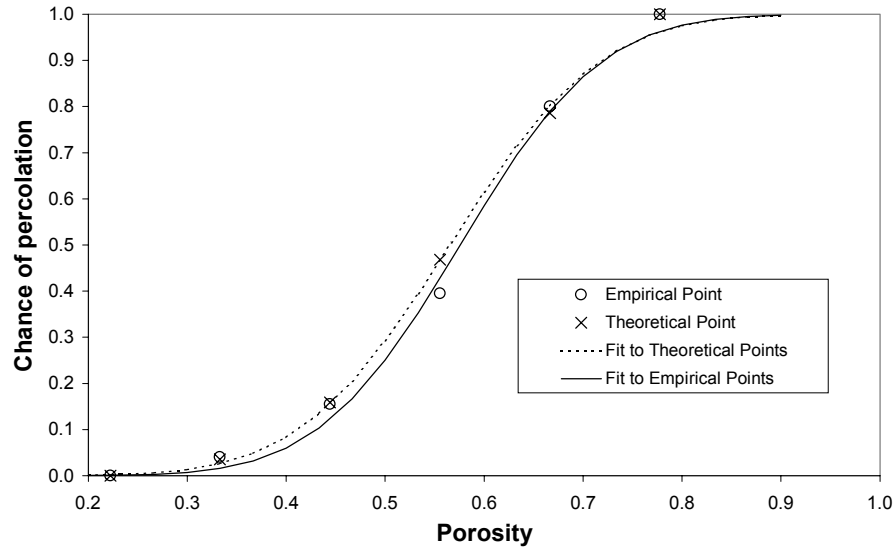


Figure 14. Fitted cumulative normal distributions for $b = 3$ and $i = 1$. Theoretical and empirical percolation probabilities.

It is clear that the cumulative normal distribution can not exactly follow the results. The tails of the distribution are asymptotic at both ends while percolation is certain or impossible when the porosity is high or low enough (see the computation of bounds below) and the distribution approaches a Heavyside function as the lattice size increases. Nevertheless, it appears to provide a reasonable basis for evaluating the results.

Figure 14 also shows theoretical points and a fitted cumulative normal distribution for the $b = 3, i = 1$ structures. The theoretical points were determined by identifying every possible configuration of pores and solids at each porosity and manually evaluating their frequency of percolation. This provided a good test of the code used to estimate the percolation frequency (the theoretical and empirical results are generally very similar) and a test of the robustness of the estimate of p_c . The fitted models in Figure 14 clearly are not identical. Nevertheless, the estimates of p_c are within 2% of each other.

Figure 15 shows the estimates of p_c computed with the Hoshen-Kopelman algorithm and the fitting procedure as implemented in this study for the Bernoulli case. The estimated percolation threshold converges towards 0.593. This suggests that the Hoshen-Kopelman code and the fitting procedure are functioning properly. The decreasing standard

deviation of the estimates with increasing b (lattice size) is a common observation [Renault, 1991].

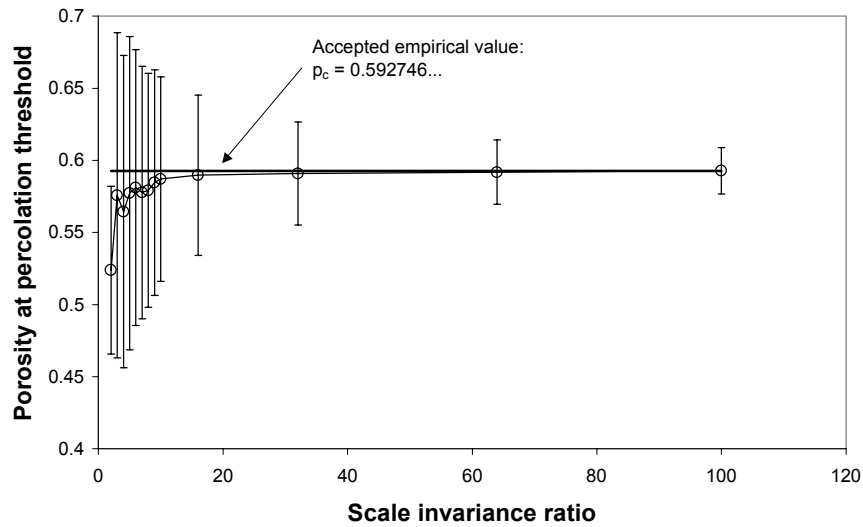


Figure 15. Percolation thresholds plus or minus the standard deviations for the first iteration level.

2.3.3 Lattice Size and Finite-Size Scaling

In finite Bernoullian systems, the correlation length ($\xi \propto |p-p_c|^{-\nu}$) of clusters at percolation is approximately equal to the lattice size L . Thus, we can set $L = \xi$, and re-arrange to solve for p_c^* , the apparent percolation threshold, as a function of L , ν , and the true p_c [Gouyet, 1996]. We have

$$p_c^* \cong p_c - CL^{-1/\nu} \quad (14)$$

with C a constant of proportionality and $\nu = 4/3$ the standard exponent that relates the correlation length to the difference $|p-p_c|$. Figure 16 shows the empirical results for the $i = 1$ lattices investigated here and a best fitting model. The fitted value of C is 0.05180....

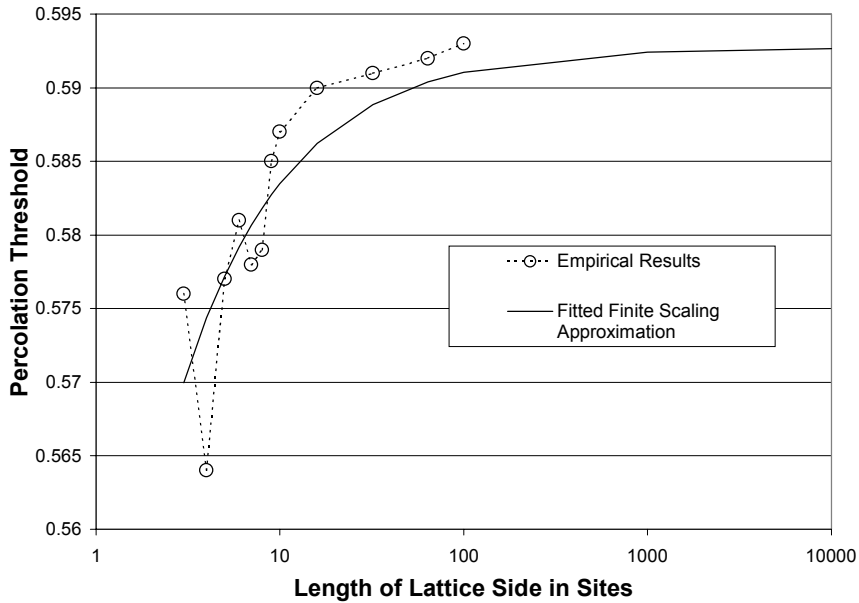


Figure 16. Finite-size effect for $i = 1$ results.

In what are believed to be the largest simulations of their kind, Jan [1999] investigated the percolation thresholds, scaling exponents, and cluster fractal dimensions in square and cubic Bernoullian site systems. For the 2-dimensional system, the lattice contained 4×10^{12} sites. The cubic lattice consisted of more than 10^9 sites. Good agreement with previous results was observed, with the 2-dimensional percolation threshold equal to 0.592746 and the fractal dimension of the clusters $D = 91/48$.

Renault [1991] considered smaller networks ranging from 125 to 10^6 sites for the three dimensional cases.

The empirical study of percolation in fractals is difficult because the number of lattice sites that must be considered increases very rapidly as a function of b and i . This limits the range of these parameters that is accessible with the computational approach utilized and the resources available.

Table 4 shows the maximum number of sites (and hence, the largest combinations of b and i) that were evaluated.

Table 4. Maximum Lattice Sizes

i	Maximum b	Number of Lattice Sites
1	100	10,000
2	16	65,536
3	10	1,000,000
4	6	1,679,616
5	4	1,048,576

2.3.4 Real Space Renormalization

Real space renormalization is a method frequently used in physics that has been applied to percolation in fractal structures [Perreau et al., 1996]. The possible configurations of occupied and unoccupied sites in a group of sites are identified. Figure 17 shows the 7 possible configurations for 4 sites [Perreau et al., 1996]. This is the 'one-cell approximation'. There are four ways in which each of the configurations of 1 and 3 occupied sites (Figure 17b and Figure 17f) can be realized, and two ways in which each of the configurations involving 2 occupied sites (Figure 17c, d, and e) can be realized. Configurations a and g have only one possible realization. In renormalization, configurations based on a through d lead to an empty site, while those based on configurations e through g give an occupied site. Note the distinction made between two occupied sites that are horizontally adjacent to one another (Figure 17d) and pairs that are vertically oriented (Figure 17e). This is related to a definition of percolation as connection between any two opposite sides of an array [Perreau et al., 1996].

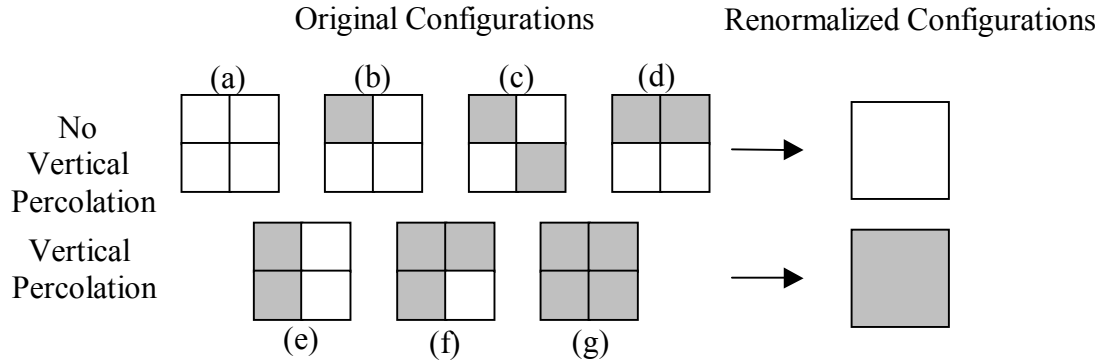


Figure 17. Renormalization for square site network. Gray sites occupied.

The renormalization function for a random 2-dimensional lattice can easily be derived. Since the independent probability of site occupation is p , the probability of two adjacent sites being occupied is p^2 , the probability of three adjacent sites is p^3 , and so on. The probability of an unoccupied site is $1-p$. Hence, 2 adjacent unoccupied sites have the probability $(1-p)^2$, three have the probability $(1-p)^3$, and so on. Combining these probabilities, we can determine the probability of each case in Figure 17:

Case a: $(1-p)^4$

Case b: $p(1-p)^3$

Cases c, d, and e: $p^2(1-p)^2$

Case f: $p^3(1-p)$

Case g: p^4

If p is the occupation probability or concentration, then the renormalized probability or concentration ϕ , after one renormalization step, is

$$\phi(p) = 2(p^2(1-p)^2) + 4(p^3(1-p)) + p^4 \quad (15)$$

where the prefactors 2 and 4 are the number of possible arrangements of 2 and 3 occupied sites (Cases e and f) and only the three cases that lead to occupied (potentially percolating) sites in the renormalized lattice are considered.

Equation (15) can be simplified to

$$\phi(p) = p^2(2 - p^2) \quad (16)$$

A fixed point of a function $f(x)$ is defined as the value at which $f(x) = x$, or equivalently $f(x) - x = 0$. In renormalization, we want the renormalized concentration $\phi(p)$ to equal the original concentration p . So, we solve for the fixed point $\phi(p) = p$. If we apply this to (16) we obtain

$$p^2(2 - p^2) - p = 0 \quad (17)$$

This has the following solutions:

$$0, 1, \frac{(\sqrt{5}-1)}{2}, \frac{(-\sqrt{5}-1)}{2} \quad (18)$$

Of these, 0 and 1 are trivial and only one of the remaining solutions is positive. This is an estimate of the percolation threshold and has the value 0.618..., which differs slightly from the value of 0.5927... estimated from numerical studies. If a similar procedure is carried out for a 3 x 3 array, the estimate of p_c is 0.609... [Turcotte, 1992]. Exact percolation thresholds are obtained for 2-dimensional bond networks and for 2-dimensional site networks on a triangular lattice [Stauffer and Aharony, 1992].

Perreau et al. [1996] used renormalization to investigate percolation of the fractal set part (the solids) of homogeneous randomized Sierpiński carpets. They investigated iteration levels from 2 through 11 explicitly and extrapolated to infinite iteration levels. Scale invariance ratios b between 4 and 64 were evaluated. Perreau et al. [1996] suggest that, because the concentration of lattice sites making up the fractal tends to 0 as the number of

fractal iterations increases, this concentration (given by $[N/b^2]^i$ and analogous to the porosity in our case) is unacceptable as a 'control' parameter for percolation on fractals. In its place, they use N/b^2 , which is simply the site occupation ratio at the first iteration and which can be conveniently converted to a fractal dimension. The results of Perreau et al. [1996] are presented in Section 2.3.5.

Renormalization can also be used to obtain estimates of the correlation length (ξ) exponent ν in $\xi = |p - p_c|^{-\nu}$, for example. At the percolation threshold, the renormalized system must have the same correlation length ξ as the original system (i.e., the system is self-similar). However, the 'lattice constant' or spacing of the renormalized lattice is different and the new correlation length is measured in the new units. Thus, if we use c as the factor relating the lattice spacing, we have

$$c|\phi - p_c|^{-\nu} = |p - p_c|^{-\nu} \quad (19)$$

Taking the logarithms of both sides yields

$$\log c - \nu \log(|\phi - p_c|) = -\nu \log(|p - p_c|) \quad (20)$$

$$\nu [\log(|\phi - p_c|) - \log(|p - p_c|)] = \log c \quad (21)$$

$$\log \frac{|\phi - p_c|}{|p - p_c|} / \log c = 1/\nu \quad (22)$$

Recognizing $(\phi - p_c)/(p - p_c)$ as the derivative $d\phi/dp$ at p_c , we arrive finally at

$$\nu = \log c / \log \frac{d\phi}{dp} \quad (23)$$

The derivative $d\phi/dp$ at p_c can be determined explicitly from (16) or its equivalent for other geometries. In this case it is $d\phi/dp = 4p - 4p^3$. At $p = p_c = 0.618\dots$ from above, the

value of the derivative is 1.527..., and, with $c = 2$ on the square lattice, $\nu = 1.635\dots$. This differs appreciably from the theoretical value of $4/3$. This renormalization procedure returns much better exponent values for 2-dimensional bond networks and for 2-dimensional site networks on a triangular lattice [Stauffer and Aharony, 1992].

2.3.5 Bounds on D_c

Mandelbrot [1983] has presented bounds on the fractal dimensions that are compatible with percolation of the fractal set. While this is not strictly applicable to our interest in pore percolation, we evaluate these bounds in relation to the renormalization results of Perreau et al. [1996] to provide a framework for the interpretation of our results.

Mandelbrot [1983] offers two conditions for an upper bound on D_c , the critical fractal dimension for percolation through the fractal set. For

$$b^E - N \geq \frac{1}{2} b^{E-1} - 1 \quad (24)$$

it is certain that percolation occurs. Note that the iteration level i does not appear in (24).

A weaker condition

$$b^E - N \geq \frac{1}{2} b^{E-1} \quad (25)$$

makes percolation 'almost' certain.

Mandelbrot's [1983] lower bound is based on p_c applied to the solids. If the first iteration results in a large enough Bernoulli lattice with a solids concentration less than p_c , then percolation is highly unlikely. Subsequent iterations remove more conducting solids and percolation becomes even less likely. In terms of fractal parameters, the solids concentration p_s can be expressed as N/b^E and, since $p_s = N/b^E > p_c$, $N > p_c b^E$. For each b , we identify a value of N (which in general is non-integer) and take the next higher integer value for the computation of the lower bound for D_c .

Figure 18 shows the weak upper bound and the lower bound together with the renormalization results of Perreau et al. [1996] as a function of b , recast as fractal dimensions using Equation (2), for different iteration levels. The results of Perreau et al. [1996] lie well within the boundaries suggested by Mandelbrot. The same results also suggest that the critical fractal dimension D_c may approach the known fractal dimension of Bernoullian percolation clusters, $D = 1.895\dots$, as the scale invariance ratio becomes large and the number of fractal iterations approaches infinity.

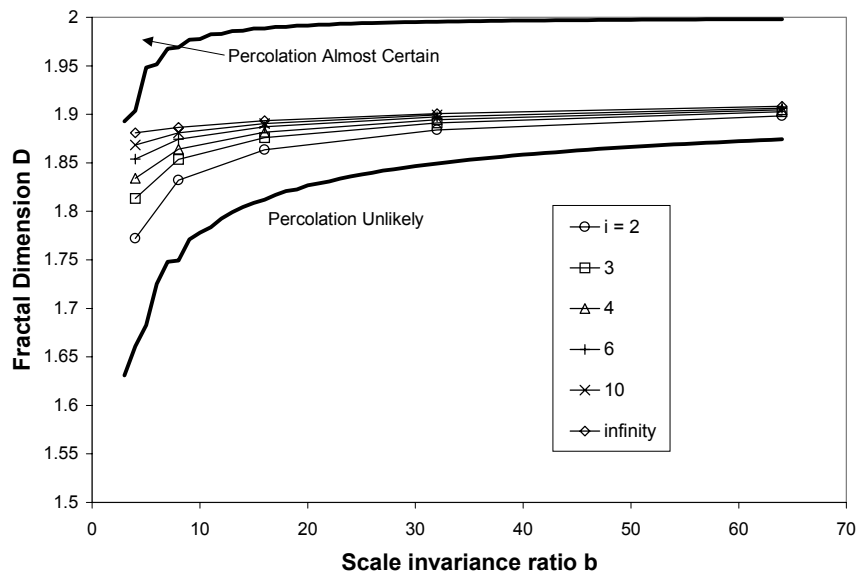


Figure 18. Mandelbrot's [1983] bounds and Perreau et al's [1996] renormalization results for percolation of the solids.

Our interest is in percolation of the complementary set. We can easily devise similar bounds on the fractal dimension (or porosity) that pertain to percolation in the pore space. As an upper bound on D we observe that the smallest number of pores that allow percolation to occur is b pores arranged in a linear fashion. No percolation is possible with $b-1$ pores. The critical value of N at which percolation cannot occur is therefore $N > b^E - b$. Because N is an integer we can write $N = b^E - b + 1$ as the smallest N at which percolation can not occur. The corresponding D_c value is $\log(b^E - b + 1)/\log(b)$.

The lower limit can be found in a similar way. As D , and hence, N , decrease, there is a point at which percolation in the pore space must occur. Figure 19 shows the maximum number of pores that can be present before the pore network percolates. Addition of one pore leads to percolation in each case. For $b > 3$, it is clear that the maximum number of pores is $(b-2)^2$ for the central pores, plus 4 for the corners, plus $2(b-2-1)$ for the edges. One more pore causes percolation. Hence $N < b^E - (b^2 - 2b + 2)$ gives a lower bound for D . Because $E = 2$ and N is integer, $N = 2b - 3$ can be related to the D_c at which percolation must occur. This lower bound applies at the first iteration level and holds for any higher iteration level.

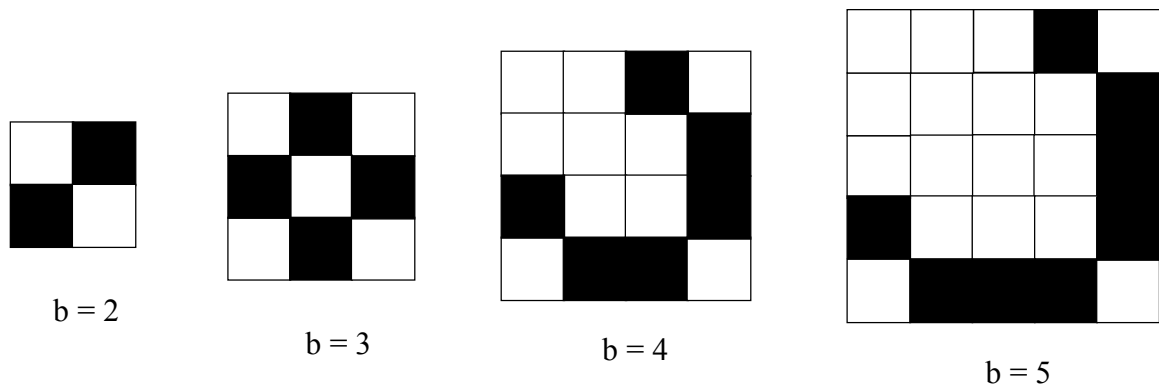


Figure 19. Maximum number of pores without pore percolation; Solids black, pores white.

An alternative bound accepts the known 2-dimensional percolation threshold for the Bernoullian lattice (0.5927...) and uses it to compute the critical fractal dimension (for $i = 1$) via rearrangement of (2). These bounds are plotted on Figure 21.

2.4 Results

2.4.1 Percolation Thresholds for Pore Space of Prefractals

In this work, it has generally been observed that it is the smaller pores that appear at higher iteration levels that are responsible for the onset of percolation in the pore space of

fractal media (Figure 20). This results in percolation clusters in which large pores are connected by small pore necks.

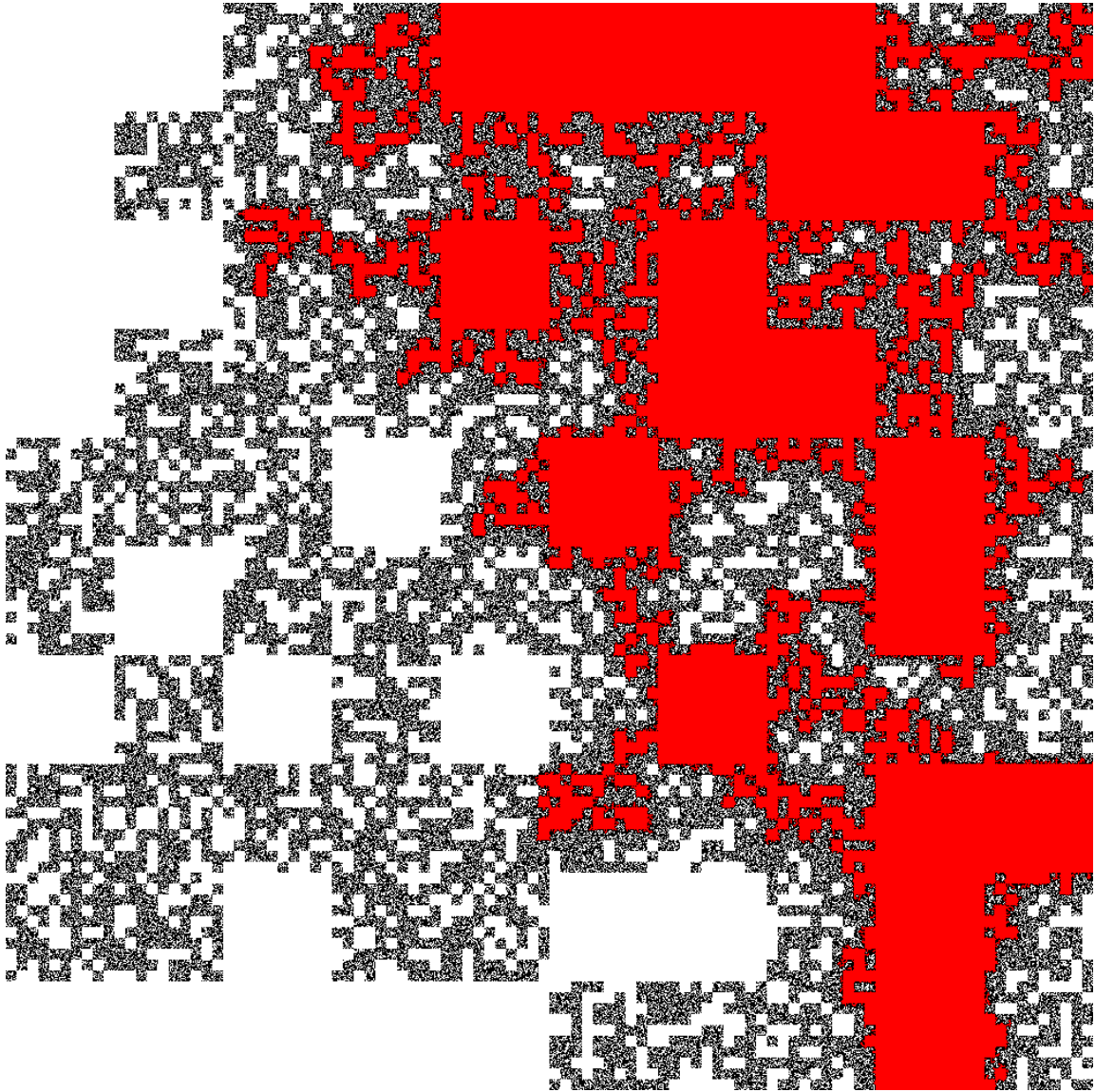


Figure 20. Percolation in the pore space of a randomized Sierpiński carpet with $b = 10$, $N = 63$, and $i = 3$ ($D = 1.799\dots$). Note that percolation in the large pores depends on the small pores. Solids black, pores connected to upper boundary that form a sample spanning cluster red, other pores white.

Figure 21 shows the bounds derived above in terms of fractal dimension. The alternative bound rapidly approaches the standard percolation threshold (all departures from this

value are due to the finite size effect, and result from the discrete nature of achievable porosities). Figure 21 also shows the empirical results generated in this study. The results are listed in Appendix C. All of the empirical results fall within the derived bounds. As the iteration level increases, the porosity increases and percolation is possible at higher fractal dimensions.

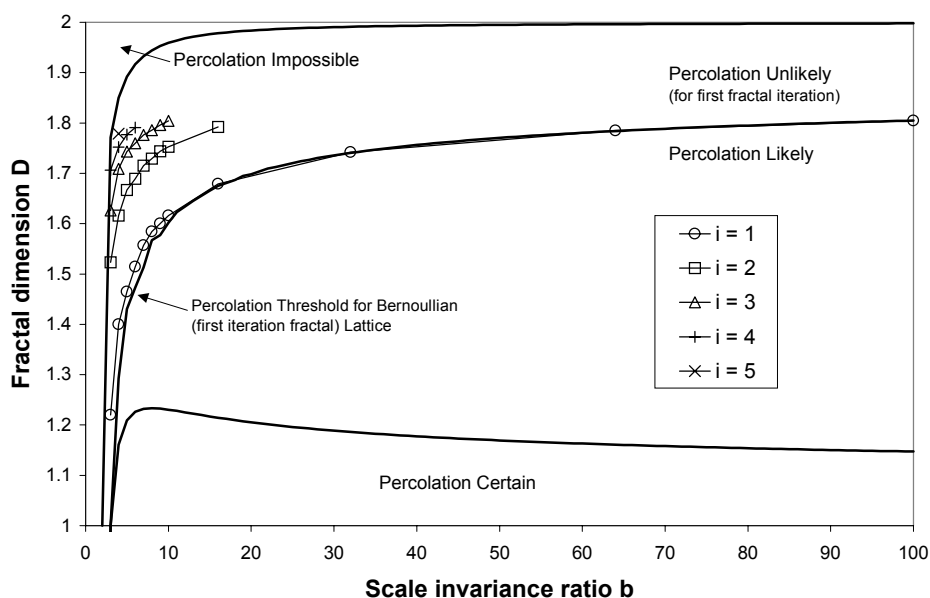


Figure 21. Upper and Lower Bounds on D_c for percolation as a function of the scale invariance ratio b and empirical results.

These results are the principal findings of this work and show a number of important behaviors. First, finite size effects appear to have a very strong impact on the critical fractal dimension for percolation until b is quite large, say 25 or perhaps 50. The utility of such large values of b in models of natural porous media is questionable. With $b = 25$, pores created at any fractal iteration have a length $1/25$ that of those created at the previous iteration. This rate of change in pore size may be excessive for many natural porous media. In my opinion, these questions have not been adequately addressed in the existing literature (see however Brakensiek and Rawls, 1992 and Tyler and Wheatcraft, 1992, which suggest b values as high as 65). For some simple fractals like the Menger sponge shown in Figure 6, it is possible to estimate the b scaling parameter by inspection.

As the value of b increases, this becomes considerably more difficult. In addition, lacunarity can obscure the relationship. In this same context, it has been proposed that the size of the largest pore relative to the size of the fractal medium be taken as a measure of b , with $b = L/r_{\max}$, where L is a linear measure of the medium size and r_{\max} is the linear size of the largest pore.

It is not difficult to investigate the parameter space for randomized sponges. The porosity ϕ of most natural soils varies between a relatively narrow range from 0.4 to 0.6 [Hillel, 1982]. Equation (2) allows computation of the fractal dimension D from ϕ , b , and i . Accepting 0.5 as a reasonable average for ϕ allows the D to be evaluated as a function of b and i only. The dependence of D on ϕ is logarithmic and hence quite small. Figure 22 shows the relationship for $2 \leq b \leq 10$ and $1 \leq i \leq 10$.

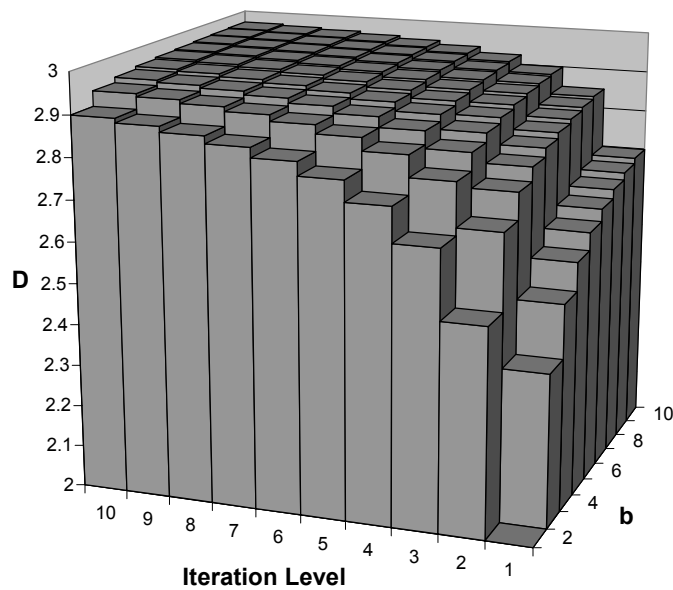


Figure 22. Fractal Dimension D as a function of b and i for 50% porosity Menger sponge.

The most important feature of this graph is that, for fixed ϕ , D rapidly approaches 3 as b and i increase. Also, it is clear that there are a number of combinations of b and i that lead to any particular D value.

If further research indicates that smaller b values are appropriate, finite size effects may have considerable importance. In addition, any models of porous media we are likely to construct using fractals in the near future will need to consider these finite size effects because of computational constraints.

The empirical results are strictly confined to the finite-size range. One approach to extrapolation of these results is presented in Figure 23. Here the critical fractal dimensions are plotted against the inverse iteration level so that extrapolation to zero corresponds to infinite iterations. Table 5 contains the linear regression coefficients and the coefficients of determination r^2 for different b values.

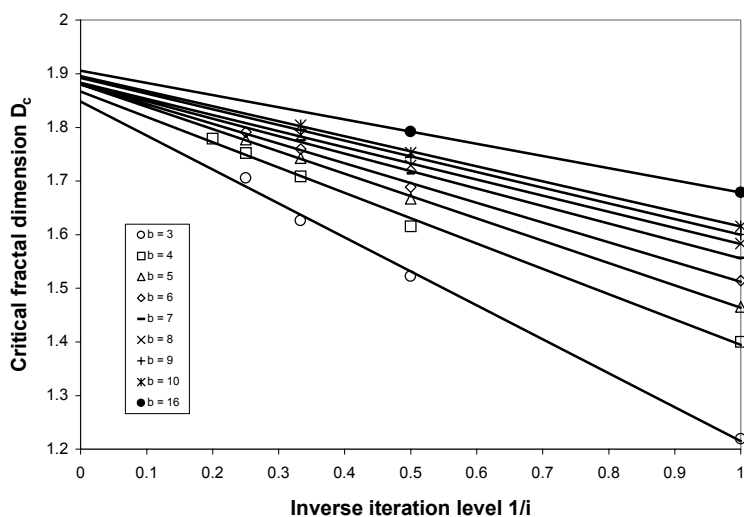


Figure 23. Relationship between D_c and inverse iteration level for different scale invariance ratios.

Table 5. Regression equations, number of points regressed (n) and coefficients of determination (r^2) for extrapolations to infinite iteration levels (Figure 23).

b	Regression Equation	n	r^2
3	$D_c = -0.6329/i + 1.8482$	4	0.9966
4	$D_c = -0.4719/i + 1.8668$	5	0.9967
5	$D_c = -0.4160/i + 1.8797$	4	0.9995
6	$D_c = -0.3680/i + 1.8802$	4	0.9983
7	$D_c = -0.3254/i + 1.8814$	3	0.9989
8	$D_c = -0.3005/i + 1.8832$	3	0.9989
9	$D_c = -0.2921/i + 1.8919$	3	0.9998
10	$D_c = -0.2803/i + 1.8956$	3	0.9994
16	$D_c = -0.2270/i + 1.9057$	2	--

A related approach is to plot D_c against $1/b$ and extrapolate to infinite scale invariance ratio. Results similar to those in Table 5 are obtained (not shown). The remarkable aspect of these results is that all of the extrapolations indicate that for $b \rightarrow \infty$ or $i \rightarrow \infty$, D_c is near 1.9 -- the fractal dimension of percolating clusters on a Bernoulli lattice. As discussed above, the results here are for percolation in the pores of fractal models of porous media of dimension D while the 'universal' D of 1.89... for Bernoulli percolation clusters pertains to the percolation cluster itself.

The results in Figure 23 and Table 5 can be used to predict the fractal dimension at the percolation threshold for any iteration level for b up to 16. Recasting the results as $1/b$ vs. D_c allows prediction for any b and for i up to 4.

From Table 5, the mean intercept (D_c) is 1.88 and its coefficient of variation is 0.8%. The intercept values show an increasing trend with increasing b . Nevertheless, the 95% confidence intervals for the intercepts always contain the established fractal dimension of 2-dimensional Bernoulli percolation clusters. Thus, based on these results we can not

reject the hypothesis that the fractal dimension of the media in which percolating clusters form at large b and i values is the same as the fractal dimension of percolating clusters in Bernoulli media. Further research is needed to determine if this conclusion holds when larger systems are incorporated into the empirical database and if it is applicable to the 3-dimensional case.

The second important feature of the empirical results in Figure 21 is the effect of iteration level. In a sense, this can also be thought of as a finite-size effect. The size of the lattice increases as b^{Ei} with increasing iteration level. Probably more significant however, is the fact that, in general, large pores generated at small iteration levels are connected by smaller pores generated at higher iteration levels, which allows percolation to occur at higher fractal dimensions.

2.4.2 Comparison with Uncorrelated Networks

It is instructive to compare these results to what is expected for uncorrelated networks. To do this we fix the porosity to the Bernoullian percolation threshold p_c and use (2) rearranged to give D as a function of i , b , E , and p_c :

$$D = \frac{\log(1 - p_c)}{i \log b} + E \quad (26)$$

This entails the assumption that the spatial structure of a fractal has no influence on its percolation behavior. For $i = 1$, this assumption is met and the equation provides a very good fit to the empirical results. For higher fractal iteration levels however, the fractal dimension predicted with (26) significantly overestimates the D at which percolation occurs (Figure 24). There is a close similarity between (26) and the regression relationships in Table 5, which can be written as $D = m 1/i + D_0$, where m is the slope and D_0 is the extrapolated y-intercept. Equation (26) has the same form with $m = \log(1 - p_c)/\log b$ and $D_0 = E$. The empirical D_0 are significantly different from $E (= 2$, in this case) however. Equation (26) is based on the assumption that $\phi = p_c$ in (2). The limit of (2) as $i \rightarrow \infty$ is $\phi = 1$. Hence, the apparent limit of Equation (26), $D = E$, may not be appropriate.

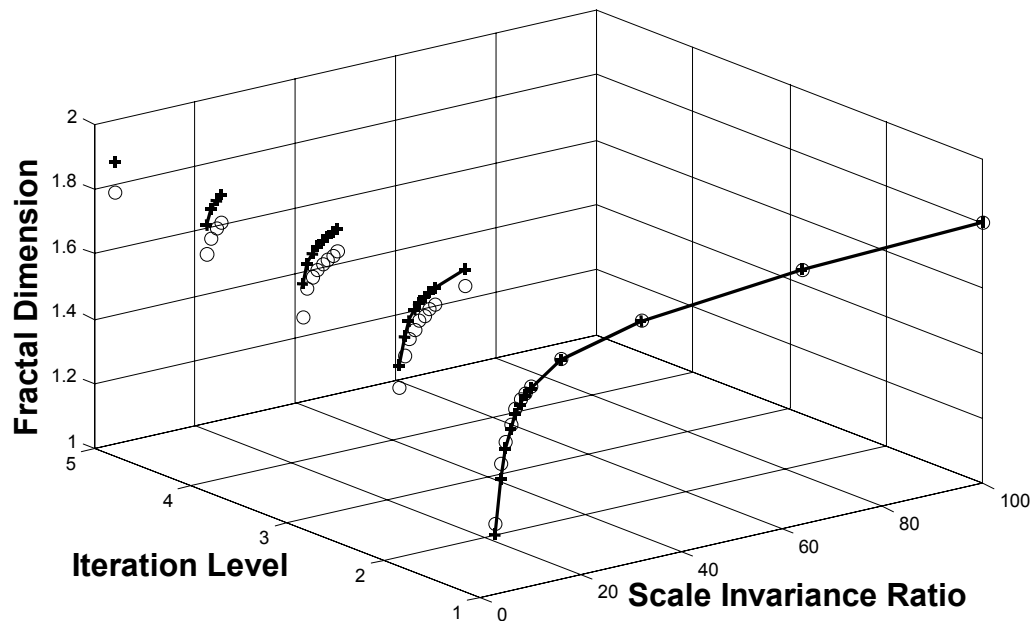


Figure 24. Empirical results (circles) and computation assuming no effect of network spatial correlation (solid lines and crosses).

We expect that similar behavior will be observed for pore percolation in 3 dimensions. Finite-scale effects will dominate the change in D_c with b until b is relatively large. The form of the dependence for the first iteration can be closely computed by simply assuming that percolation occurs at p_c as we have done for the 2-dimensional case in Figure 21 and Figure 24. Similarly, Equation (26) can also be used to compute curves like those in Figure 24, and a similar departure of the actual critical D values from them is expected as a result of the prefractal's correlation structure. It is expected that large pores generated at low iteration levels will be connected by smaller pores generated at higher iteration levels.

2.4.3 Comparison with Dye Staining Images and Pore Networks from Thin Sections

A number of scientists have contributed to the understanding of the movement of chemicals in porous media by capturing the spatial distribution of surface-applied dye in the profile following infiltration [Flury et al., 1994; Perillo et al., 1999; Schwartz et al.,

1999]. In general, complex patterns reminiscent of percolation clusters are obtained, especially under drier initial conditions. Perillo et al. [1999] refer to such staining patterns as 'intricately dyed zones' and were not able to attribute them to soil features they could observe.

The direct description of pore space by thin section preparation is also an important area of endeavor and provides insight into the spatial organization and connectivity of pores.

The results of such studies give us an opportunity to qualitatively evaluate which types of percolation clusters -- standard Bernoullian fractal clusters (Figure 11) or those that arise in fractal porous media (Figure 20) -- may be more appropriate models, at least for certain types of pore space and for the combined phenomena that lead to the actual dye staining patterns in a particular soil. To this end, a portion of a dye-staining image [Schwartz et al., 1999] and a binary soil photomicrograph [Ringrose-Voase, 1987] are compared with each type of cluster in Figure 25. Clearly, the two types of artificial percolation clusters are significantly different. In addition, the dye-staining image distinctly reveals the 3-dimensional nature of the process that generated it as there is a significant disconnection between dyed areas. In fact, many stained areas are completely isolated from other stained areas in this 2-dimensional section. Similarly, there is no need for the pore space to be connected in the plane of the thin section. This is a significant limitation for the comparison of the clusters generated in 2-dimensional media with the dye-staining patterns and the pore space image, which are 2-dimensional sections of 3-dimensional systems. It can only be resolved by extending the work described here to 3 dimensions. Nevertheless, my impression is that the pore cluster model (lower right) is superior to the Bernoulli cluster model for the simulation of the particular dye staining and pore space images in Figure 25. This is in agreement with the findings of Crawford and Matsui [1996] that it is the solids rather than the pores of natural porous media that follow fractal scaling.

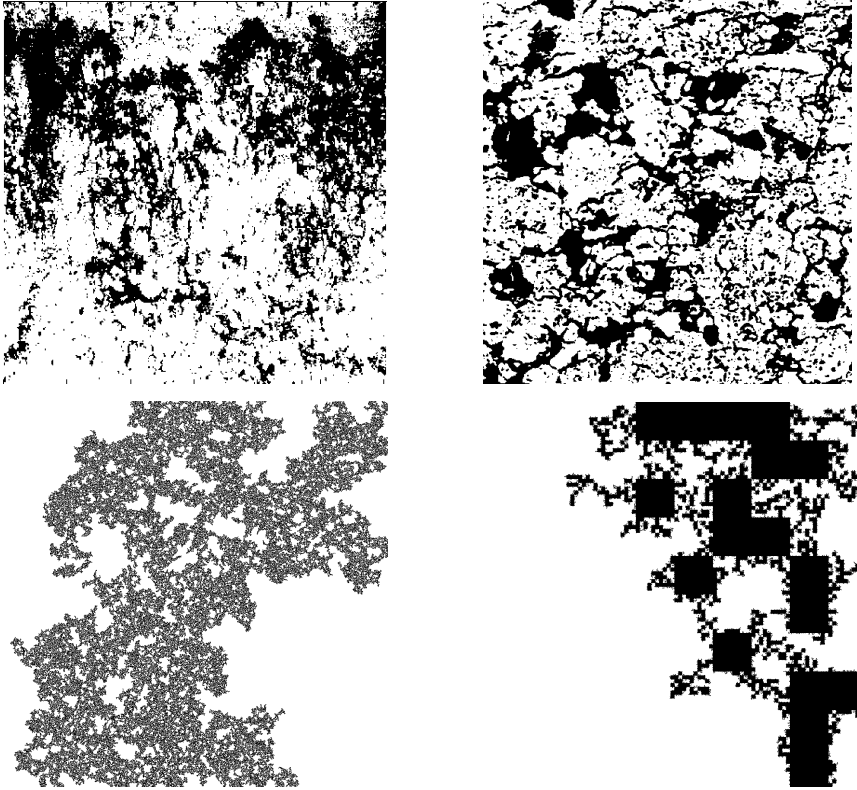


Figure 25. Comparison of a portion of a soil dye-staining image (top left; approximately 40x40 cm, Costa Rican ultisol ; Schwartz et al., 1999; $D = 1.79$), thin section image (top right) [Ringrose-Voase, 1987], Bernoullian percolation cluster (bottom left; $D = 1.839\dots$), and percolation cluster in fractal porous medium (bottom right; porous medium $D = 1.799\dots$).

2.5 Conclusions

Bernoullian site percolation clusters are known to be fractal and can be approximated by prefractal models. However, percolation in the pore space of mass prefractal porous medium models has not been previously investigated. Such media are popular as models of porous media. Empirical simulation of 2-dimensional prefractal porous media and determination of their percolation thresholds reveals strong finite size effects and important fractal iteration level effects; at the percolation thresholds, larger pores generated by lower iteration levels are generally connected by smaller pores generated at

higher iteration levels. This results in a network of large pore bodies connected by small pore necks.

These results should prove valuable for the prediction of the onset of percolation in models of prefractal porous media. The results can be used to bound modeling efforts. Percolation phenomena have application to a number of research areas relevant to porous media [Sahimi, 1994]. The results here may also have more fundamental application in fluid flow problems and other areas. Although only a limited range of parameters has been explored empirically, extrapolations allow estimates of the critical fractal dimension to be made for a larger number of combinations of iteration level and scale invariance ratio. It is also likely that results similar to those observed here will apply to the 3-dimensional case.

Extrapolation of the empirical results to infinite iterations suggests that there may be a unique fractal dimension of the solid matrix at which the pore space first percolates. The fractal dimension at which this occurs appears to be around 1.9 -- close to the universal fractal dimension of Bernoullian site percolation clusters. Similar behavior might be found for the 3-dimensional case.

Percolation clusters that form in prefractal porous media are considerably different from those that form in a Bernoulli lattice. The clusters formed within prefractal media appear to be better models of clusters that exist in many real pore spaces because they have large pore bodies connected by small pore necks. Comparison of the percolation clusters in the pores of prefractal porous media with thin section images of natural porous media and soil dye-staining images suggests that these models may be appropriate for the simulation of pore space and transport phenomena.

This work should be extended, both in the range of parameters evaluated for the 2-dimensional case and into 3 dimensions. A 3-dimensional model is necessary for comparison with real processes in porous media.

Chapter 3. Application to Soil Water Retention

3.0 Summary

This chapter synthesizes the results of Chapters 1 and 2 in an application to soil water retention in random fractal porous media models. Previous applications of fractal scaling to soil water retention are reviewed and problems with models that do not consider a minimum pore size are exposed. An application to soil water retention that was originally computed with the less desirable algorithm is re-calculated and compared with the original. This re-calculation resulted in a unique pore size distribution and more uniform water retention curves. It is demonstrated that constructing fractal porous media with the heterogeneous algorithm leads to substantially greater variability in water retention than is observed in media constructed with the homogeneous algorithm. Findings on the percolation thresholds for pore percolation in the random fractal models from Chapter 2 are shown to differentiate between well-connected systems where existing simple models of water retention in fractal porous media give reasonable predictions, and poorly connected systems where these models fail.

3.1 Previous Applications of Fractal Scaling to Soil Moisture Retention

Perhaps the first paper that made use of a fractal approach to quantifying the soil moisture retention is that of Ahl and Niemeyer [1989]. They arrived at $V_p \propto \psi^{D-3}$ where V_p is the cumulative pore volume. This is equivalent to the Campbell model [Campbell, 1985]

$$\frac{\theta}{\phi} = \left(\frac{\psi}{\psi_0} \right)^{\frac{1}{b}} \quad (27)$$

with $D-3 = -1/b$ or $D = 3 - 1/b$, where θ is the volumetric water content, ψ is the matric potential, and ψ_0 is the air-entry matric potential. Ahl and Niemeyer [1989] computed D

in the range 2.1 to 2.84 for 11 soils. They found the highest D values in surface horizons. They also pointed out an intuitive reason why D approaches 3 in some soils; the pore volume 'penetrates' the sample space completely and is nearly space-filling.

Tyler and Wheatcraft [1989] used parameters determined from a fractal interpretation of particle size data to estimate a parameter in a previously empirical model of soil water retention.

In 1990, the same authors published the first paper that explicitly used a fractal model of pore space. They used Sierpiński carpet-type constructions and related the carpets' water retention properties to the parameters of Brooks and Corey and the Campbell empirical water retention models. They showed that, relative to their planar carpet model, clayey soils had fractal dimensions approaching 2 while sandy soils had fractal dimensions closer to 1.

Rieu and Sposito [1991a,b,c] followed with papers that arrive at the following equation for a fragmented fractal porous medium:

$$\psi = \psi_0 [(1 - \phi) + \theta]^{1/D-3} \quad (28)$$

For 6 soils, D was found to range between 2.758 and 2.968, with finer textured soils yielding higher values.

3.2 Alternative Derivation of Fractal Water Retention Model

The equation developed by Al and Niemeyer [1989] and its relationship to the Campbell [1985] model demonstrated by Tyler and Wheatcraft [1989] suffer from a failure to include both upper and lower scaling limits. Without a lower scaling limit, Menger sponge-type models ultimately reach 100% porosity as fractal iterations continue indefinitely.

The relationship between the Campbell [1985] model and the model of Ahl and Niemeyer [1989] is demonstrated by an alternative approach here. This derivation makes the principal shortcoming of the Ahl and Niemeyer [1989] model (lack of lower scaling limit) plain. The next section presents a model that explicitly incorporates a lower scaling limit.

The Campbell [1985] model for soil water retention can be written as

$$\theta = \phi \left(\frac{\psi}{\psi_0} \right)^{-\frac{1}{b}} \quad (29)$$

Because ψ_0 and ϕ are constants, they can be combined into a constant k :

$$\theta = k(\psi)^{-\frac{1}{b}} \quad (30)$$

Assuming capillary behavior, the matric potential is given by the Young-Laplace equation

$$\psi = \frac{-2\sigma \cos \alpha}{\rho_w r} \quad (31)$$

where r is the radius of a cylindrical pore, and α is the wetting contact angle. Assuming perfect wetting ($\alpha = 0$ and $\cos \alpha = 1$), substituting (31) into (30), and combining the factor -2, the surface tension σ , the density of water ρ_w , and the previous constant k into k' , gives

$$\theta = k' \left(\frac{1}{r} \right)^{-\frac{1}{b}} \quad (32)$$

The volumetric water content is defined as the volume of water V_w divided by the total volume V_t

$$\theta = \frac{V_w}{V_t} \quad (33)$$

Equating the right hand sides of (32) and (33) and incorporating the constant V_t into k'' yields

$$V_w = k'' \left(\frac{1}{r} \right)^{\frac{1}{b}} \quad (34)$$

In the pore space of a fractal, there are essentially three ways the numbers of pores and solids can be counted. The most familiar counting of the fractal set, or the 'solids' as used here, is $N = r^{-D}$, where N is the number of cubes of size r needed to cover the set. For example, for the Menger sponge (Figure 6), there are $N = 20$ 'solids' of size $1/3$ and $N = 400$ 'solids' of size $1/9$. These 'solids' are fictitious however in that they are 'full of holes' and do not directly account for the volume or mass of the fractal porous medium. The number N_p of pores or gaps also follows a scaling rule of the form $N_p \propto r^{-D}$. So for example, the Menger sponge has 7 pores of size $1/3$ and 140 pores of size $1/9$. Because N_p is not cumulative, it is not useful in the current context. The third way of counting the pores is to take the difference between the number of solids that would occupy the total volume of the porous medium (N_T) and the number of quasi-solids N . This number $N_p' = N_T - N = r^{-E} - N$ (or $N_p' = r^{-3} - N$ in 3-dimensional space), has the properties that it gives the total number of pores (including those of larger size) measured in units of size r . For example, the Menger sponge has 7 pores of size $1/3$, but it has a total number of $N_p' = 729 - 400 = 329$ 'pores' (i.e., pore space) measured in cubes of size $1/9$.

The volume of water contained in N_p' cubical pores of size r is

$$V = N_p' r^3 \quad (35)$$

Cylindrical pores of radius r and height r would contain $V = N_p' \pi r^3$. Thus, the constant π (or other shape-dependent factor) is immaterial.

V_w in Equation (34) represents the total volume of fluid retained in a porous medium in all pore sizes from r to some minimum r . It can be written as $V_w = V_{wT} - V$, where V_{wT} is the volume of water contained in the porous medium at saturation. V_{wT} can also be evaluated using Equation (35) in the limit of the minimum r : $V = N_p' r^3 = (r^{-3} - N)r^3 = 1 - Nr^3 = 1 - r^{-D}r^3 = 1 - r^{3-D}$. Because $3 - D > 0$, the limit of $V = 1 - r^{3-D}$ as $r \rightarrow 0$ is $V = V_{wT} = 1$. This indicates that the porosity is 100% and should not be a surprising result. The entire volume of the unit volume porous medium is pore space because a minimum $r > 0$ is not specified in this model. This shows a significant flaw in any similar fractal model that does not incorporate a minimum pore size.

Now we can proceed with the derivation. Using $V_w = V_{wT} - V$, Equation (35), and the result $V_{wT} = 1$, we have $V_w = 1 - N_p' r^3 = 1 - (r^{-3} + N)r^3 = Nr^3$.

Substitution into (34) gives

$$Nr^3 = k \left(\frac{1}{r} \right)^{\frac{1}{b}} \quad (36)$$

Rearranging as

$$N = k \left(\frac{1}{r} \right)^{\frac{1}{b}} \left(\frac{1}{r} \right)^3 \quad (37)$$

and

$$N = k \left(\frac{1}{r} \right)^{3 - \frac{1}{b}} \quad (38)$$

Finally,

$$N = k'' r^{-\left(3-\frac{1}{b}\right)} \quad (39)$$

This is equivalent to the fundamental fractal power law $N \propto r^{-D}$ with $D = 3 - 1/b$. Based on this relation, $D - 3 = -1/b$ and substitution into (29) yields

$$\theta = \theta_s \left(\frac{\psi}{\psi_0} \right)^{D-3} \quad (40)$$

This result is the same as that of Ahl and Neimeyer [1989] and related to that of Perfect [1999] (see below).

3.3 Three Parameter Model

Perfect [1999] proposed a 3-parameter model that included the fractal dimension, an upper scaling limit (related to the air entry tension), and a lower scaling limit (related to the tension at complete dryness).

Perfect [1999] makes a number of important assumptions to apply a Menger sponge-like model to soil water retention curves. First, all pores are hydraulically connected to the atmosphere by larger pores. This ensures that progressively smaller pores can desaturate as the soil moisture tension increases. This appears to be the case for the non-random Menger sponge (Figure 6). However, it is easy to imagine randomized sponges that will violate this assumption and the results presented in Chapters 1 and 2 demonstrate the lack of connectivity and its impact. A second important assumption is that pores completely dewater when the tension needed to drain cylindrical pores of 'equivalent' radii is reached. This neglects the existence of wetting films and fluid 'wedges' that can be held in pore corners.

Following Rieu and Sposito [1991a, b, c] and Perfect [1999], the volumetric water content of a sponge constructed to the i^{th} level as the j^{th} iteration level pores drain is given by

$$\theta_{j,i} = b^{j(D-3)} - b^{i(D-3)} \quad (41)$$

Because we already know the water content at saturation (equal to the porosity) from (2), we can compute the relative saturation $Sw = \theta_{j,i}/\phi$ as

$$Sw = \frac{b^{j(D-3)} - b^{i(D-3)}}{1 - b^{i(D-3)}} \quad (42)$$

Now, from the capillary equation, the tension is inversely proportional to the pore size r . Because $r_1 = (1/b)^1$ at the first iteration level (where the largest pores appear), the air-entry tension ψ_0 is proportional to $1/r_1$ or b^1 . Generalizing to other tensions and sizes, we can write

$$\psi_{i-1} \propto b^i \quad (43)$$

Next, we determine the ratio of the tension to the tension at air-entry as

$$\frac{\psi_i}{\psi_0} = \frac{b^{i+1}}{b^1} = b^i \quad (44)$$

Finally, we insert (44) into (42) and, after a small amount of re-arrangement, arrive at [Perfect, 1999]

$$Sw = \frac{\psi_j^{D-3} - \psi_i^{D-3}}{\psi_0^{D-3} - \psi_i^{D-3}} \quad (45)$$

which applies for $\psi_0 \leq \psi_j \leq \psi_i$. Here ψ_i is a constant equal to the tension that drains the smallest pores. ψ_0 is the tension that drains the largest pores. ψ_j is the tension applied to the porous medium. For application of this equation to real soils, Perfect [1999] considers ψ_j a continuous variable. For our immediate purposes working with known fractal models however, it suffices to retain ψ_j in its original form. Figure 26 shows the

water retention function for a range of fractal dimensions when the largest and smallest pore sizes remain the same ($\psi_o = 0.1$ kPa and $\psi_i = 100$ kPa, respectively).

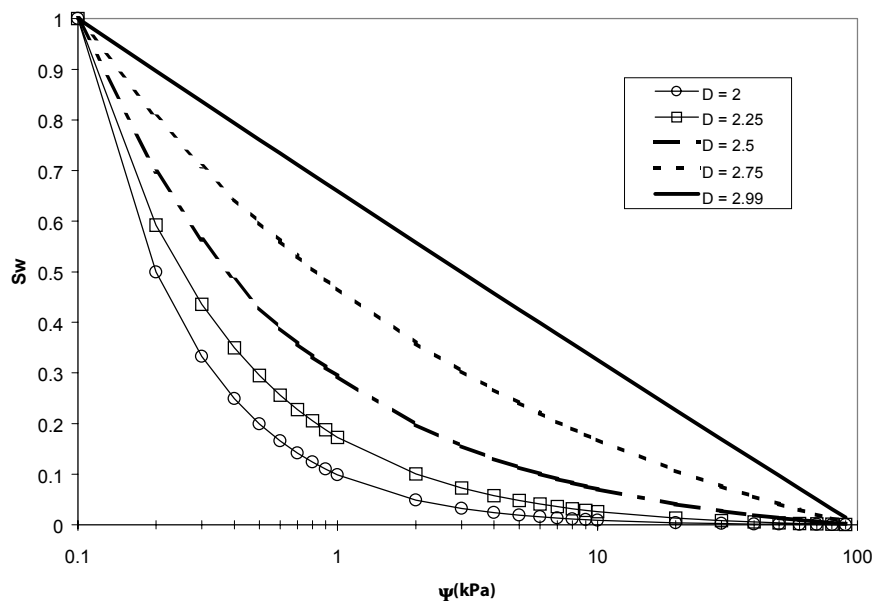


Figure 26. Perfect [1999] model for soil water retention in fractal pore space.

Like other models of soil water retention in prefractal pore spaces, this model assumes all water is held by capillary forces in accordance with the Young-Laplace equation.

Comparison of the predictions of this model with network and lattice gas simulations of retention in non-random prefractals like the Menger sponge that meet its other assumptions (particularly the assumptions about connectivity and coalescence of pores) may allow the impact of the strictly capillary assumption to be isolated and identified.

3.4 Previous Work on Pore Connectivity and Coalescence in Fractal Water Retention Models

In perhaps the first paper to explicitly consider the effects of pore connectivity on water retention in a prefractal model of porous media, Bird and Dexter [1997] computed moisture-tension relations in 2-dimensional prefractal pore networks. They simulated drainage in $b = 3$, $i = 5$ randomized Sierpiński carpets (generated with the heterogeneous algorithm with $p = 0.7, 0.8,$ and 0.9) by allowing three sides of the prefractal structure to be open to the atmosphere while the bottom was connected to a water sink. At a given

tension, all pores of size greater than r that are filled with water and are connected to the atmosphere by at least one path consisting of pores no smaller than r , drain. Note that this approach also neglects the coalescence of pores that in reality can lead to pores larger than any particular size r computed from the fractal scaling equations. For example, consider the largest pore of Figure 4, which is enlarged relative to the $1/3 \times 1/3$ size produced by the fractal generating process as a result of its connection to other pores.

The tension at which a pore drains completely is taken as inversely proportional to the size r , as it is in the Young-Laplace equation. This approach is therefore similar to most others in its assumption of purely capillary behavior. The approach is different from most others however, in that it considers the pore connectivity.

Bird and Dexter [1997] used the heterogeneous algorithm and presented simulated water retention curves for a number of different porosities ranging from 0.41 to 0.97. These are theoretical porosity values according to Equation (5). The actual porosities vary as demonstrated above. As an introduction to the impact of the different algorithms, we focus our attention on structures similar to their first three examples ($p = 0.7, 0.8,$ and 0.9) where porosity ranges from 0.41 to 0.83. The computer code used by Bird and Dexter [1997] was modified to generate homogeneous porous media for comparison. Later, we compare the results of water retention simulations in 1000 realizations of heterogeneous and homogeneous for each of 3 values of p .

Figure 27 through Figure 29 compare water retention simulations on prefractal media generated using the homogeneous algorithm with those on media built with the heterogeneous algorithm. The solid probability p decreases in the sequence of figures. S is the relative saturation and $\log_b \psi$ is the scaled log of tension derived as follows: As noted above, r depends on b as $r = (1/b)^i$ where i is the iteration. Because $\psi \propto 1/r \propto b^i$ in the Young-Laplace equation (Equation (31)), taking logarithms yields $\log \psi \propto i \log b$, or $\log_b \psi \propto i$. Hence, $\log_b \psi$ can be represented by the prefractal's iteration i . 'Pore Size Curves' shown on the figures indicate water retention and drainage in all pores,

irrespective of their connectivity. For the homogeneous algorithm, these are equivalent to the Perfect [1999] water retention model, which is described in detail in Section 3.3.

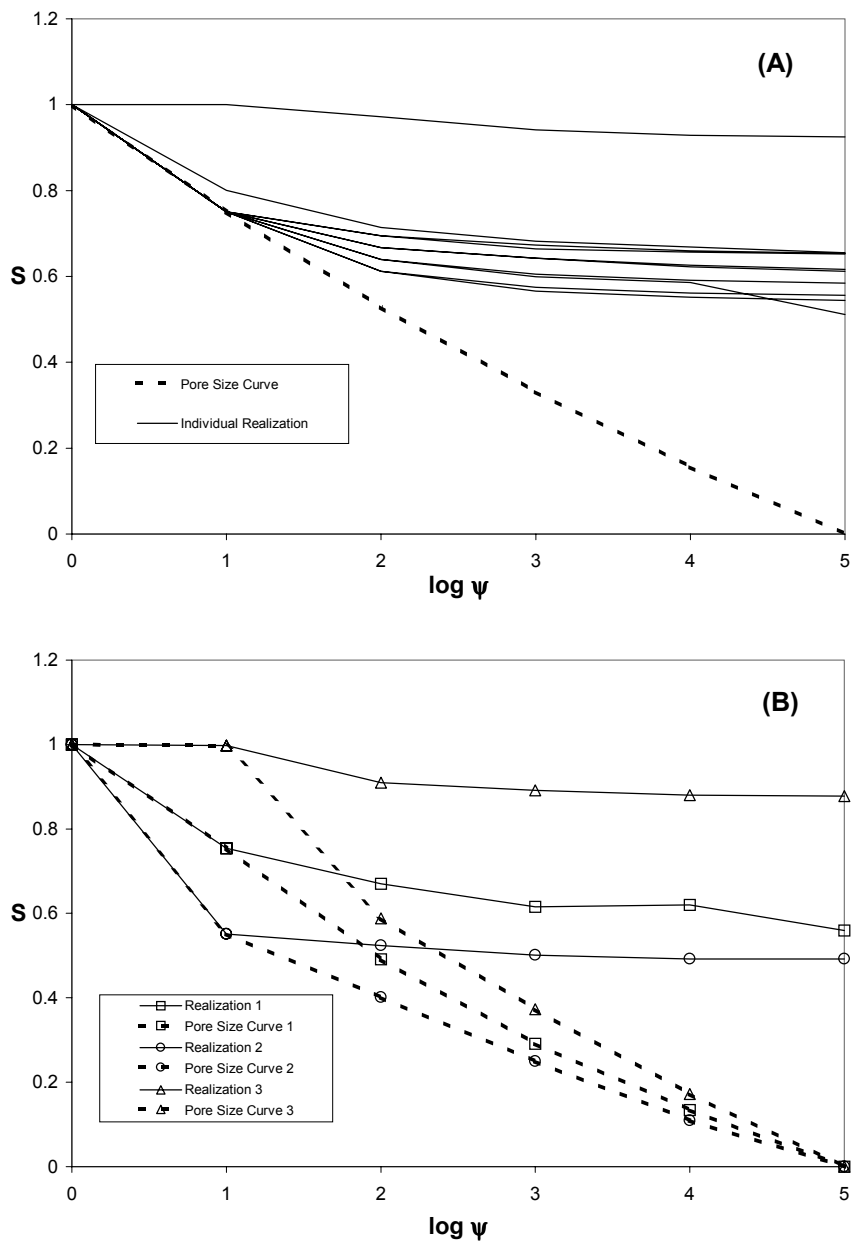


Figure 27. Impact of different algorithms on simulated water retention: (A) homogeneous, $p=8/9$, (B) Heterogeneous, $p=0.9$. Heterogeneous results from Bird and Dexter [1997], Figure 3.

Clearly, the impact of incomplete pore connectivity is to inhibit complete drainage. This causes the water retention curves to deviate from the 'pore size' curves. The deviation is more pronounced at higher p values (lower porosities) because connectivity increases as porosity increases. Chapter 2 considers the connectivity as a function of fractal dimension, b value, and iteration level in detail.

The single homogeneous realization that differs significantly from the others in Figure 27A is due to the case where the large pore generated during the first iteration occupies the center of the carpet and is not connected to a path that permits it to drain at higher tensions. The same phenomenon could also occur with the heterogeneous algorithm. However, despite the similarity of the retention curve in Figure 27B, Realization 3, it is clear from the 'pore size' curve that no large pore was formed by the heterogeneous algorithm in that realization (Figure 27B, Pore Size Curve 3). In contrast, Realization 1 of the heterogeneous results in Figure 28B is due to isolation of a large pore. This pore is connected to the atmosphere via smaller pores and ultimately drains.

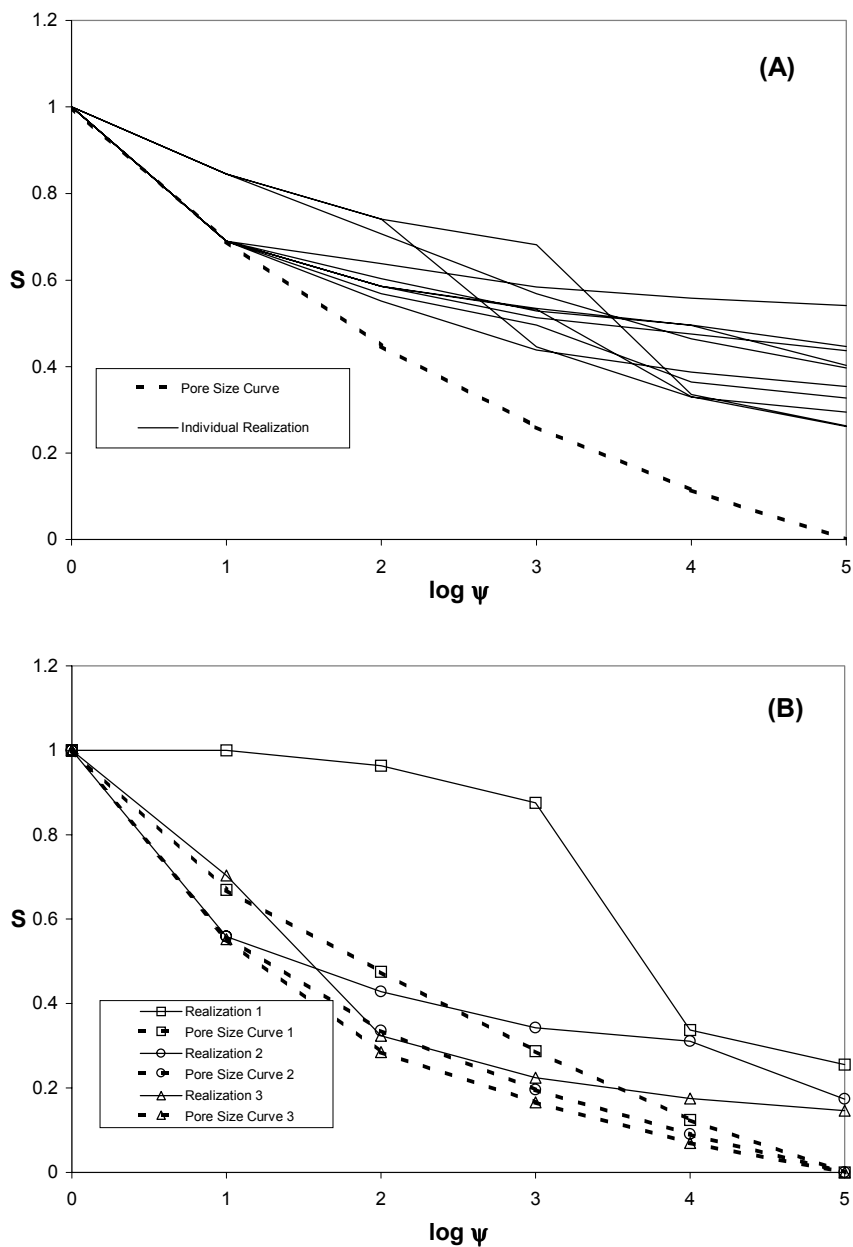


Figure 28. Impact of different algorithms on simulated water retention: (A) homogeneous, $p=7/9$, (B) heterogeneous, $p=0.8$. Heterogeneous results from Bird and Dexter [1997], Figure 3.

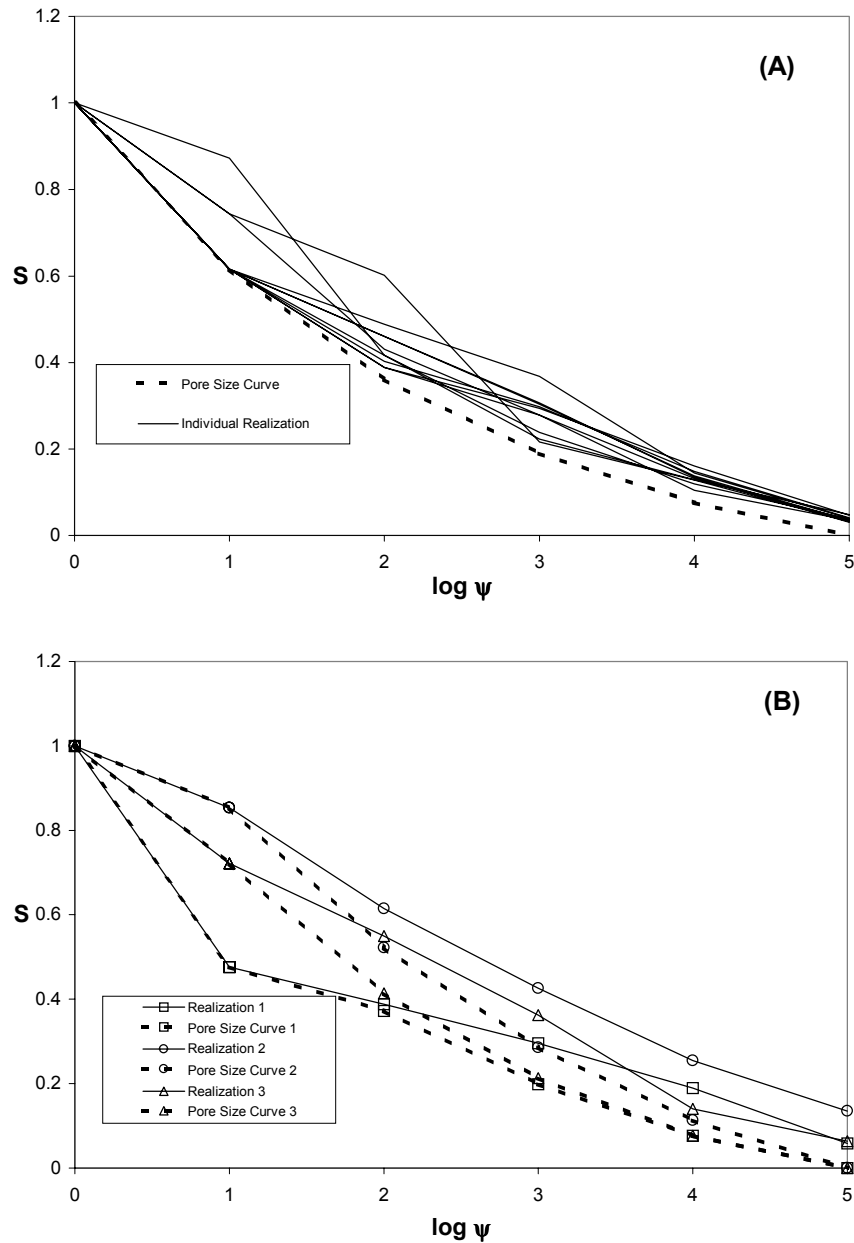


Figure 29. Impact of different algorithms on simulated water retention: (A) homogeneous, $p=6/9$, (B) heterogeneous, $p=0.7$. Heterogeneous results from Bird and Dexter [1997], Figure 3.

These figures reveal two important distinctions between the fractal algorithms. First, there is only one pore size distribution (when the coalescence of pores is neglected) and hence, only one porosity associated with the homogeneous algorithm for a particular set

of prefractal parameters. As a result of the heterogeneous algorithm, each realization of the porous prefractal has a different pore size curve and porosity. Second, there is in general less variability in the computed drainage curves for the homogeneous algorithm. This means that the effect of pore connectivity, for a particular set of prefractal parameters, is better elucidated by the simulated water retention on the structures generated with the homogeneous algorithm.

Figure 30 through Figure 32 compare water retention simulations on prefractal media generated with the homogeneous and heterogeneous algorithms at three different p values using the method of Bird and Dexter [1997]. The p values, $6/9$, $7/9$, and $8/9$, were selected to maintain a reasonable range of porosities. The Equation (5) porosities range from 45 to 87%.

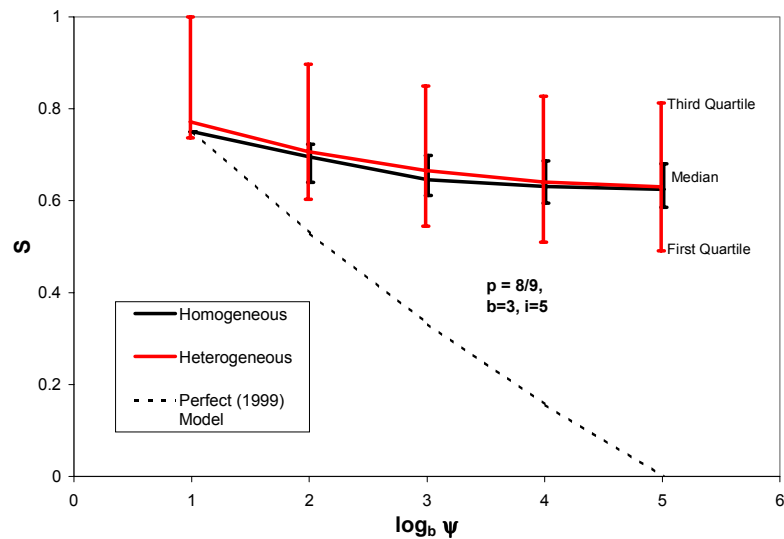


Figure 30. Impact of homogeneous and heterogeneous fractal-generating algorithms on simulated water retention for 1000 realizations of 2-dimensional $b = 3$, $i = 5$ prefractal porous media with $p=8/9$.

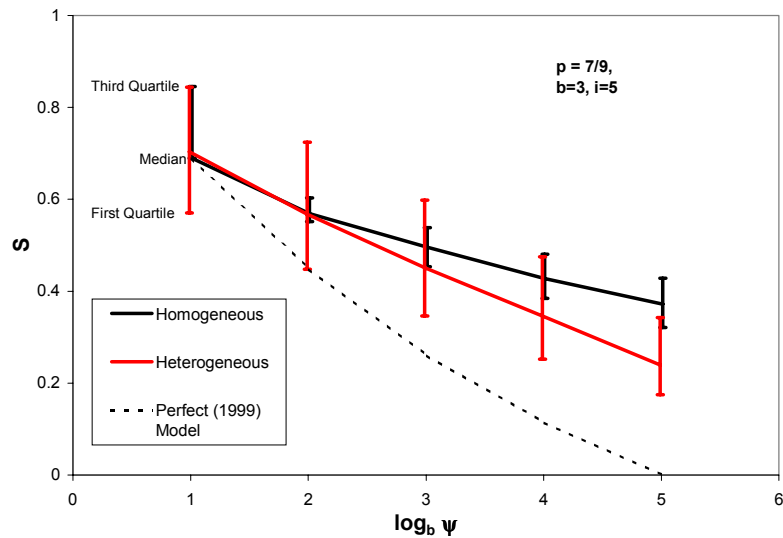


Figure 31. Impact of homogeneous and heterogeneous fractal-generating algorithms on simulated water retention for 1000 realizations of 2-dimensional $b = 3, i = 5$ prefractal porous media with $p=7/9$.

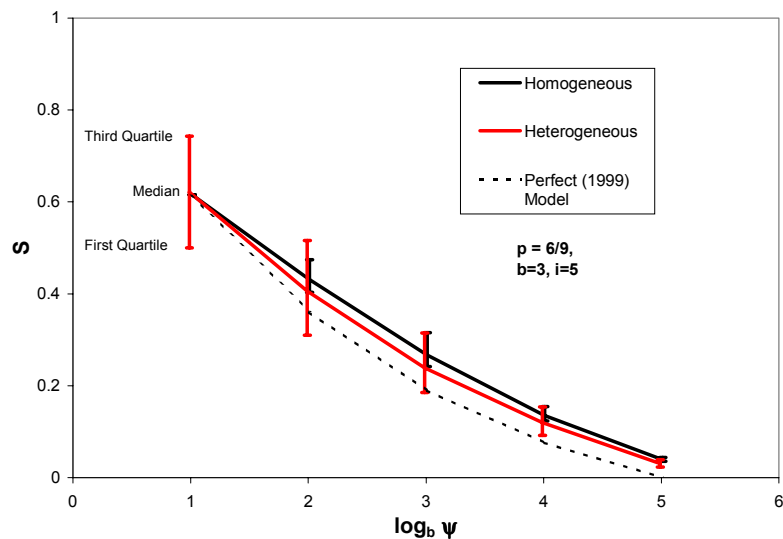


Figure 32. Impact of homogeneous and heterogeneous fractal-generating algorithms on simulated water retention for 1000 realizations of 2-dimensional $b = 3, i = 5$ prefractal porous media with $p=6/9$.

Figure 30 through Figure 32 emphasize the important distinctions in the behavior of media generated with the different fractal algorithms; there is in general less variability in the computed drainage curves for the structures generated with the homogeneous algorithm. This must be the case because all homogeneous structures belong to a subset of the possible heterogeneous structures.

The distributions of simulated water saturations around their median value as a function of applied tension were highly non-normal for both homogeneous and heterogeneous prefractals. Therefore, we use non-parametric statistics to summarize the results. The principal findings are that the range of saturations between the first and third quartiles for water retention in heterogeneous prefractal structures was on average more than twice as large as that for homogeneous prefractals (Table 6). Thus, the effects of pore connectivity on water retention for a particular set of prefractal parameters can be better elucidated by the less-variable structures generated with the homogeneous algorithm.

Table 6. Ratio of interquartile ranges of saturation for heterogeneous and homogeneous algorithms at each tension for varying p . ($3^{\text{rd}}-1^{\text{st}}$ quartiles heterogeneous/ $3^{\text{rd}}-1^{\text{st}}$ quartiles homogeneous).

$\log_b \psi$	$p=8/9$	$7/9$	$6/9$
1	∞^1	1.76	∞^1
2	3.52	5.33	2.90
3	3.53	2.98	1.75
4	3.43	2.33	2.01
5	3.39	1.58	1.96

¹Interquartile range of homogeneous results = 0

The deviation in the median saturations for the homogeneous and heterogeneous algorithms when $p = 7/9$ (Figure 31) can likely be attributed to the percolation properties of the pore networks in the fractal media [Chapter 2 and Sukop et al., 2001b]. When $p = 8/9$, percolation cannot readily occur in either the heterogeneous or homogeneous

networks and saturation remains high over all tensions. When $p = 6/9$, percolation occurs easily. For the intermediate $p (= 7/9)$, percolation is hindered in the homogeneous case, which always maintains its fractal dimension $D = 1.77\dots$, but occurs frequently in the heterogeneous case where more than 20% of the time the realized dimension of the first iteration structure is $D = 1.63\dots$, lower than the critical fractal dimension for percolation in these structures ($D = 1.716\dots$) [Chapter 2 and Sukop et al., 2001b].

Figure 30 through Figure 32 also show the results of the Perfect [1999] model (Equation (45)). At high p values, the computed saturations considering pore connectivity differ significantly from those predicted by this model. This model is based on the assumptions of purely capillary behavior and complete connectivity. If these assumptions are met, ψ_i in Equation (45) is determined by the smallest pore size. In randomized prefractal media however, pore connectivity is usually incomplete and dryness cannot be achieved at any tension if pores containing water are isolated. This is most significant when the connectivity of the pore network is low (i.e., when the fractal dimension of the medium is high and the porosity is low). Figure 30 shows that, due to pore isolation, little and eventually no reduction in saturation occurs when tension is increased. The optimal ψ_d is therefore infinite. At lower p values (higher porosity, Figure 32), the Perfect model works significantly better.

3.4 Conclusions

Bird and Dexter [1997] conclude that, within certain parameter ranges, pore connectivity can make it impossible to accurately measure the pore size distribution from the water retention curve. The algorithmic differences in assigning pores do not have a substantial impact on this conclusion, but it is shown here that the reduced variability associated with the homogeneous random fractal algorithm seems preferable for the investigation of hydrologic processes in fractal porous media. It is also shown here that the parameter ranges where pore size distributions can be measured can be predicted based on the percolation thresholds determined in Chapter 2.

Appendices

Appendix A: Random Sierpiński Carpet Generator

```

% M. Sukop, 2001. MATLAB V. 5.3
% Program computes, displays, and stores randomized Sierpinski Carpets.
% The homogeneous or heterogeneous (binomial/truncated binomial) algorithms
% can be specified.
% b is fractal scaling parameter (3 for standard Sierpinski Carpet).
% p is the probability of a pore at each iteration level (1/9 for standard carpet).
% Output is to file Junk.bmp ('truecolor') or to Junk.dat,
% which is either ARCINFO-compatible Grid ASCII file
% or ASCII file of x and y coordinates and 1's (solids) or 0's (pores)
% in the following order:
% row 1, column 1;
% row 1, column 2; ...

clear
rand('state',sum(100*clock))

typemode=input('Select fractal type: 0 = homogeneous; 1 = heterogeneous; 2 = non-random ')

if typemode < 2

b=input('b value ? ')
p=input('p (pore probability) value ? ')

end

maxit=input('Maximum number of iterations ? ')

if typemode == 1

    hettypemode=input('Select heterogeneous mode: 0 = regular binomial; 1 = truncated binomial ')

elseif typemode == 2

a=input('Specify generator; e.g., [0 0 0, 0 1 0, 0 0 0] for standard Sierpinski carpet: ')
b=sqrt(length(a))
p=sum(a)/length(a)

```

```

end

n=round(b^2-p*b^2)
D=log(n)/log(b)

outmode=input('Select output mode:...0 = GRIDASCII; 1 = X,Y ASCII; 2 = BMP(truecolor) ')

it=1
if typemode==0 %Homogeneous Algorithm

    a=randperm(b^2);
    for i = 1:b^2;
        if a(i)<=n
            c(i)=uint8(0);%solid - black
        else
            c(i)=uint8(255);%pore - white
        end
    end
end

elseif typemode==1 %Heterogeneous Algorithm

    if hettypemode==0 %Regular binomial

        a=rand(b^2,1);
        for i = 1:b^2;
            if a(i)<=1-p
                c(i)=uint8(0);
            else
                c(i)=uint8(255);
            end
        end
    end

    else %Truncated binomial
        a=2;
        while min(a)>1-p
            a=rand(b^2,1);
        end
    end
end

```

```

        for i = 1:b^2;
            if a(i)<=1-p
                c(i)=uint8(0);
            else
                c(i)=uint8(255);
            end
        end
    end
end

else %non-random
    c=uint8(255*a);
end %end algorithm selection

for row=1:b;
    for col=1:b;
        d(row,col)=c(row*b-(b-col));
    end;
end;

oldcol=1
while it<maxit
    for oldrow=1:b^it;
        disp(100*oldrow*oldcol/b^(2*it))
        disp('% done current iteration')
        for oldcol=1:b^it;
            if d(oldrow,oldcol)==uint8(255)%if pore
                for newrow=oldrow*b-(b-1):oldrow*b;
                    for newcol=oldcol*b-(b-1):oldcol*b;
                        e(newrow,newcol)=uint8(d(oldrow, oldcol));
                    end
                end
            end
        end
    end
else

if typemode==0 %Homogeneous Algorithm

        a=randperm(b^2);
        for i = 1:b^2;

```

```

        if a(i)<=n
            c(i)=uint8(0);%solid - black
        else
            c(i)=uint8(255);%pore - white
        end
    end
end

elseif typemode==1 %Heterogeneous Algorithm

    if hettypemode==0 %Regular binomial

        a=rand(b^2,1);
        for i = 1:b^2;
            if a(i)<=1-p
                c(i)=uint8(0);
            else
                c(i)=uint8(255);
            end
        end
    end

    else %Truncated binomial
    a=2;
    while min(a)>1-p
        a=rand(b^2,1);
    end

        for i = 1:b^2;
            if a(i)<=1-p
                c(i)=uint8(0);
            else
                c(i)=uint8(255);
            end
        end
    end

end

else %non-random
    c=uint8(255*a);
end %end algorithm selection

```

```

        newrow=oldrow*b-(b-1);
        newcol=oldcol*b-(b-1);
        for row=1:b;
            for col=1:b;
                e(newrow+row-1,newcol+col-1)=uint8(c(row*b-(b-col)));
            end
        end
    end
end
end
end
it=it+1
d=uint8(e);
end
clear e;

if outmode==1
    %generate output arrays
    for i=1:(b^it);
        disp(100*i/b^it)
        disp('% done building x and y vectors')
        for j=1:(b^it);
            x((i-1)*b^it+j)=(2*i-1)/(2*b^it);
            y((i-1)*b^it+j)=1-(2*j-1)/(2*b^it);
        end
    end
    end
    disp('Reshaping and transposing')
    z=double(reshape(d,b^(2*it),1));
    z=z/255;
    z=1-z; %exchange 1 and 0 ('solids' = 1)
    x=x';
    y=y';
    out=[x y z];
    disp('writing file')
    save junk.dat out -ascii;

elseif outmode==0
    %generate gridascii output

```

```

z=double(d);
z=z/255;
z=1-z; %exchange 1 and 0 ('solids' = 1)

fid=fopen('junk.dat','w');
fprintf(fid,'NCOLS %g',b^it);
fprintf(fid,'\rNROWS %g',b^it);
fprintf(fid,'\rXLLCORNER %g',0);
fprintf(fid,'\rYLLCORNER %g',0);
fprintf(fid,'\rCELLSIZE %g',1/b^it);
fprintf(fid,'\rNODATA_VALUE %g',9999);
for i=1:b^it;
    fprintf(fid,'\r');
    fprintf(fid,'%2.0g',z(i,:));
end
status=fclose(fid);

elseif outmode==2
%bmp1 output
e(:,1)=d;
e(:,2)=d;
e(:,3)=d;
imwrite(e,'junk.bmp')

viewmode=input('View bmp file?: 0 = No; 1 = Yes ')

    if viewmode==1
        image(imread('junk.bmp'))
        axis('equal')
    end
end

```


Appendix B: Random Menger Sponge Generator

```

% M. Sukop, 2001. MATLAB V. 5.3
% Program computes, displays, and stores randomized Menger Sponges.
% The homogeneous or heterogeneous (binomial/truncated binomial) algorithms
% can be specified.
% b is fractal scaling parameter (3 for standard Menger Sponge).
% p is the probability of a pore at each iteration level (7/27 for standard sponge).
% Output to Junk.dat is ASCII file of x,y, and z coordinates and 1's (solids) or 0's (pores)
% in the following order:
% row 1, column 1, layer 1;
% row 1, column 1, layer 2; ...

clear
rand('state',sum(100*clock))

b=input('b value ? ')
p=input('p value ? ')
n=round(b^3-p*b^3)

D=log(n)/log(b)

maxit=input('Maximum number of iterations ? ')
typemode=input('Select fractal type: 0 = homogeneous; 1 = heterogeneous; 2 = non-random ')

if typemode == 1

        hettypemode=input('Select heterogeneous mode: 0 = regular binomial; 1 = truncated
binomial ')

elseif typemode == 2

        a=input('Specify generator; e.g., [1 1 1, 1 0 1, 1 1 1, 1 0 1, 0 0 0, 1 0 1, 1 1 1, 1 0 1, 1 1 1] for
standard Menger sponge')
end
it=1
if typemode==0 %Homogeneous Algorithm
a=randperm(b^3);
for i = 1:b^3;

```

```

        if a(i)<=n
            c(i)=1;%solid
        else
            c(i)=0;%pore
        end
    end
end
elseif typemode==1 %Heterogeneous Algorithm
if hettypemode==0 %Regular binomial
    a=rand(b^3,1);
    for i = 1:b^3;
        if a(i)<=1-p
            c(i)=1;
        else
            c(i)=0;
        end
    end
end

else %Truncated binomial
    a=2;
    while min(a)>1-p
        a=rand(b^3,1);
    end
    for i = 1:b^3;
        if a(i)<=1-p
            c(i)=1;
        else
            c(i)=0;
        end
    end
end

end
else %non-random
c=a;
end %end algorithm selection
for row=1:b;
    for col=1:b;
        for lay=1:b;
            d(row,col,lay)=c(row*b^2-(b^2-b*col)-(b-lay));

```

```

end;
end;
end;
oldcol=1
while it<maxit
    for oldrow=1:b^it;
        disp(100*oldrow*oldcol/b^(2*it))
        disp('% done current iteration')
        for oldcol=1:b^it;
            for oldlay=1:b^it;
                if d(oldrow,oldcol,oldlay)==0
                    for newrow=oldrow*b-(b-1):oldrow*b;
                        for newcol=oldcol*b-(b-1):oldcol*b;
                            for newlay=oldlay*b-(b-
1):oldlay*b;
                                e(newrow,newcol,newlay)=d(oldrow,oldcol,oldlay);
                                    end
                                end
                            end
                        end
                    end
                else
                    if typemode==0 %Homogeneous Algorithm
                        a=randperm(b^3);
                        for i = 1:b^3;
                            if a(i)<=n
                                c(i)=1;
                            else
                                c(i)=0;
                            end
                        end
                    end
                    elseif typemode==1 %Heterogeneous Algorithm
                        if hettypemode==0 %Regular binomial
                            a=rand(b^3,1);
                            for i = 1:b^3;
                                if a(i)<=1-p
                                    c(i)=1;
                                else

```

```

                                                    c(i)=0;
                                                    end
                                                end
                                            else %Truncated binomial
                                                a=2;
                                                while min(a)>1-p
                                                    a=rand(b^3,1);
                                                end
                                                for i = 1:b^3;
                                                    if a(i)<=1-p
                                                        c(i)=1;
                                                    else
                                                        c(i)=0;
                                                    end
                                                end
                                            end
                                        end
                                    end
                                else %non-random
                                    c=a;
                                end %end algorithm selection

                                newrow=oldrow*b-(b-1);
                                newcol=oldcol*b-(b-1);
                                newlay=oldlay*b-(b-1);
                                for row=1:b;
                                    for col=1:b;
                                        for lay=1:b;
                                            e(newrow+row-1,newcol+col-1,newlay+lay-1)=c(row*b^2-(b^2-b*col)-(b-lay));
                                        end
                                    end
                                end
                            end
                        end
                    end
                end
            end
        end
    end
end
it=it+1
d=e;
end

```

```

close
figure(1)
hold on
fid = fopen('junk.dat','w');
col=0;
for row=1:b^maxit;
    disp(100*row*col/b^(2*it))
    disp('% done generating plot')
    for col=1:b^maxit;
        for lay=1:b^maxit;
            if d(row,col,lay)==1;
                xmin=(row-1)/b^maxit;
                xmax=row/b^maxit;
                ymin=(col-1)/b^maxit;
                ymax=col/b^maxit;
                zmin=lay/b^maxit;
                zmax=(lay-1)/b^maxit;

                fprintf(fid,'%6.5f %6.5f %6.5f \n',xmin+(xmax-xmin)/2,ymin+(ymax-ymin)/2,zmin+(zmax-
zmin)/2); vert=[xmin,ymin,zmin;xmax,ymin,zmin; xmax,ymax,zmin; xmin,ymax,zmin; xmin,ymin,zmax;
xmax,ymin,zmax; xmax,ymax,zmax; xmin,ymax,zmax];
                fac=[1 2 6 5; 2 3 7 6; 3 4 8 7; 4 1 5 8; 1 2 3 4; 5 6 7 8];
                rgbcolors=[1 1 0; 0 1 0; 1 1 0; 0 1 0; 0 0 1; 0 0 1];
                patch('faces',fac,'vertices',vert,'FaceVertexCData',rgbcolors,'FaceColor','flat','EdgeColor',[1 1
1],'BackFaceLighting','reverselit');
            view(3)
            end;
        end;
    end;
end;
fclose(fid)
light('Position',[-1,0,0]);
%light('Position',[0,-1,0]);
%light('Position',[0,0,1]);
hold off

```

Appendix C: Porosity (ϕ), Standard Deviation of Porosity (σ), and Fractal Dimension (D) at the Percolation Threshold for Different Iteration Levels and Scale Invariance Ratios

i	b	ϕ	σ	D
1	2	-	-	-
1	3	0.576	0.113	1.220
1	4	0.564	0.108	1.400
1	5	0.577	0.109	1.465
1	6	0.581	0.096	1.514
1	7	0.578	0.087	1.557
1	8	0.579	0.081	1.584
1	9	0.585	0.078	1.600
1	10	0.587	0.071	1.616
1	16	0.590	0.056	1.679
1	32	0.591	0.036	1.742
1	64	0.592	0.022	1.785
1	100	0.593	0.016	1.805
2	3	0.650	0.084	1.523
2	4	0.655	0.076	1.616
2	5	0.657	0.069	1.667
2	6	0.672	0.067	1.689
2	7	0.671	0.063	1.715
2	8	0.676	0.055	1.729
2	9	0.675	0.052	1.744
2	10	0.680	0.054	1.753
2	16	0.684	0.048	1.792
3	3	0.708	0.060	1.626
3	4	0.702	0.059	1.709
3	5	0.711	0.049	1.743

3	6	0.725	0.046	1.760
3	7	0.729	0.041	1.776
3	8	0.737	0.034	1.786
3	9	0.740	0.033	1.796
3	10	0.742	0.033	1.804
4	3	0.726	0.047	1.706
4	4	0.747	0.045	1.752
4	5	0.762	0.032	1.777
4	6	0.776	0.031	1.791
5	4	0.784	0.024	1.779

References

- Adler, P.M. and J.-F. Thovert, Fractal porous media, *Transport in Porous Media*, 13, 41-78, 1993.
- Ahl, C. and J. Niemeyer, The fractal dimension of the pore-volume inside soils, *Z. Pflanzenernahr. Bodenk*, 152, 457-458, 1989.
- Benzi, R. G. Paladin, G. Parisi, and A. Vulpiani, On the multifractal nature of fully developed turbulence and chaotic systems, *J. Phys. A: Math. Gen.*, 17, 3521-3531, 1984.
- Berkowitz, B. and I. Balberg, Percolation theory and its application to groundwater hydrology, *Wat. Resour. Res.* 29, 775-794, 1993.
- Berkowitz, B. and R.P. Ewing, Percolation theory and network modeling applications in soil physics, *Surveys in Geophys.* 19, 23-72, 1998.
- Bird, N.R.A. and A.R. Dexter, Simulation of soil water retention using random fractal networks, *Euro. J. Soil Sci.*, 48, 633-641, 1997.
- Bird, N.R.A., E. Perrier, and M. Rieu, The water retention function for a model of soil structure with pore and solid fractal distributions, *Euro. J. Soil Sci.* 51, 55-63, 2000.
- Bird, N.R.A., F. Bartoli, and A.R. Dexter, Water retention models for fractal soil structures. *Euro. J. Soil Sci.*, 47, 1-6, 1996.
- Brakensiek, D.L. and Rawls, W.J., Comment on "Fractal processes in soil water retention" by Scott W. Tyler and Stephen W. Wheatcraft, *Wat. Resour. Res.* 28, 601-601, 1992.

Brooks, R.H. and A.T. Corey, Hydraulic properties of porous media, *Hydrology Paper 3*, 22-27, Colorado State University, Fort Collins, Colorado, 1964.

Bunde, A. and S. Havlin (Eds.), *Fractals and disordered systems*, Springer-Verlag, Berlin, 1996.

Campbell, G.S., *Soil physics with BASIC*, Elsevier Science Publishers, Amsterdam, 1985.

Chayes, J.T. and L. Chayes, The large-N limit of the threshold values in Mandelbrot's fractal percolation process, *J. Phys. A: Math. Gen.* 22, L501-L506, 1989.

Chayes, J.T., L. Chayes, and R. Durrett, Connectivity properties of Mandelbrot's percolation process, *Prob. Th. Rel. Fields* 77, 307-324, 1988.

Chayes, L., Aspects of the fractal percolation process, *Progress in Probability* 37, 113-143, 1995.

Crawford, J.W. and I.M. Young. The interactions between soil structure and microbial dynamics, in *Fractals in Soil Science*, edited by P. Baveye, J.-Y Parlange, and B.A. Stewart, pp. 233-260, CRC Press, Boca Raton, 1998.

Crawford, J.W., and N. Matsui, Heterogeneity of the pore and solid volume of soil: distinguishing a fractal space from its non-fractal complement, *Geoderma* 73, 183-195, 1996.

Crawford, J.W., K. Ritz, and I.M. Young, Quantification of fungal morphology, gaseous transport and microbial dynamics in soil: an integrated framework utilising fractal geometry, *Geoderma*, 56, 157-172, 1993.

Crawford, J.W., P. Baveye, P. Grindrod, and C. Rappoldt, Application of fractals to soil properties, landscape patterns, and solute transport in porous media, in *Assessment of*

non-point source pollution in the vadose zone, Geophysical monograph, 108, pp. 151-164, American Geophysical Union, 1999

Crawford, J.W., The relationship between structure and the hydraulic conductivity of soil, *Euro. J. Soil Sci.*, 45, 493-502, 1994.

Duckers, L.J., Percolation with nearest neighbor interaction, *Physics Letters 67A*, 93-94, 1978.

Duckers, L.J. and R.G. Ross, Percolation with non-random site occupation, *Physics Letters 49A*, 361-362, 1974.

Dullien, F.A.L., Characterization of porous media - pore level, *Transport in Porous Media 6*, 581-606, 1991.

Evertsz, C.J.G. and B.B. Mandelbrot, Multifractal measures. in *Fractals and Chaos*, edited by Peitgen, H-O., H. Jurgens, and D. Saupe, Springer-Verlag, New York. 921-969, 1992.

Feder, J., *Fractals*, Plenum Press, New York, 1988.

Flury, M., H. Fluhler, W.A. Jury, and J. Leuenberger, Susceptibility of soils to preferential flow of water: a field study, *Wat. Resour. Res.* 30, 1945-1954, 1994.

Freund, J.E. *Mathematical Statistics*. 463 pp. Prentice-Hall Inc. Engelwood Cliffs, New Jersey, 1971.

Geffen, Y., A. Aharony, and B.B. Mandelbrot, Phase transitions on fractals: I. Quasi-linear lattices, *J. Phys. A: Math. Gen.* 16, 1267-1278, 1983.

Geffen, Y., A. Aharony, Y. Shapir, and B.B. Mandelbrot, Phase transitions on fractals: II. Sierpiński gaskets, *J. Phys. A: Math. Gen.* 17, 435-444, 1984a.

Geffen, Y., A. Aharony, and B.B. Mandelbrot, Phase transitions on fractals: III. Infinitely ramified lattices, *J. Phys. A: Math. Gen.* 17, 1277-1289, 1984b.

Gouyet, J-F., *Physics and fractal structures*, 234 pp., Springer, New York, 1996.

Hillel, D., *Introduction to soil physics*. Academic Press, Inc., Orlando FL, 1982.

Jan, N., Large lattice random site percolation. *Physica A* 226, 72-75, 1999.

Lin, Z-Q. and Z.R. Yang, Thresholds and universality of the site percolation on Sierpiński carpets, *Commun. Theor. Phys.* 27, 145-152, 1997.

Machta, J., Phase transitions in fractal porous media, *Phys. Rev. Lett.* 66, 169-172, 1991.

Mandelbrot, B.B., Intermittent turbulence in self-similar cascades: divergence of high moments and dimension of the carrier, *J. Fluid Mech.* 62, 331-358, 1974.

Mandelbrot, B.B., Negative fractal dimensions and multifractals. *Physica A*, 163, 306-315, 1990.

Mandelbrot, B.B., Random multifractals: negative dimensions and the resulting limitations of the thermodynamic formalism. *Proc. R. Soc. Lond. A* 434, 79-88, 1991.

Mandelbrot, B.B., *The fractal geometry of nature*, W.H. Freeman and Co., New York, 1983.

Mani, V. and K.K. Mohanty, Effect of pore-space spatial correlations on two-phase flow in porous media, *J. Petrol. Sci. Engr.* 23, 173-188, 1999.

Muller, J., Characterization of pore space in chalk by multifractal analysis. *J. Hydrol.*, 187, 215-222, 1996.

Nauman, E. B., Cocontinuity and Percolation in Correlated Structures, *AIChE Symposium Series 89*, 134-142, 1993.

Odagaki, T., H. Kawai, and S. Toyofuku, Percolation in correlated systems, *Physica A* 266, 49-54, 1999.

Paladin, G. and A. Vulpiani, Anomalous scaling laws in multifractal objects. *Phys. Rep.*, 156, 147-225, 1987.

Patil, G.P., Maximum likelihood estimation for generalized power series distributions and its application to a truncated binomial distribution, *Biometrika* 49, 227-237, 1962.

Perfect, E., Estimating soil mass fractal dimensions from water retention curves, *Geoderma*, 88, 221-231, 1999.

Perillo, C.A., S.C.Gupta, E.A. Nater, J.F. Moncrief, Prevalence and initiation of preferential flow paths in a sandy loam with argillic horizon, *Geoderma* 89, 307-331, 1999.

Perreau, M., J. Peiro, and S. Berthier, Percolation in random-Sierpiński carpets: A real space renormalization group approach, *Physical Review E* 54, 4590-4595, 1996.

Perrier, E., C. Mullon, M. Rieu, G. de Marsily, Computer construction of fractal soil structures: simulation of their hydraulic and shrinkage properties, *Water Resour. Res.*, 31, 2927-2943, 1995.

Perrier, E., M. Rieu, G. Sposito, G. de Marsily, Models of the water retention curve for soils with a fractal pore size distribution, *Water Resour. Res.*, 32, 3025-3031, 1996.

Perrier, E., N. Bird, and M. Rieu, Generalizing the fractal model of soil structure: the pore-solid fractal approach, *Geoderma*, 88, 137-164, 1999.

Rappoldt, C. and J.W. Crawford, The distribution of anoxic volume in a fractal model of soil, *Geoderma*, 88, 329-347, 1999.

Renault, P., The effect of spatially blocking-up of some bonds or nodes of a network on the percolation threshold, *Transport in Porous Media* 6, 451-468, 1991.

Rieu, M. and E. Perrier, Fractal models of fragmented and aggregated soils, in *Fractals in Soil Science*, edited by P. Baveye, J.-Y Parlange, and B.A. Stewart, pp. 169-202, CRC Press, Boca Raton. 1998.

Rieu, M. and G. Sposito, Fractal fragmentation, soil porosity, and soil water properties: 1. Theory, *Soil Sci. Soc. Am. J.*, 55, 1231-1238, 1991a.

Rieu, M. and G. Sposito, Fractal fragmentation, soil porosity, and soil water properties: 2. Applications, *Soil Sci. Soc. Am. J.*, 55, 1239-1244, 1991b.

Rieu, M. and G. Sposito, The water characteristic curve of fragmented porous media and the fractal nature of soil structure, *C. R. Acad. Sci. Paris*, 312, 1483-1489, 1991c.

Ringrose-Voase, A.J., A scheme for the quantitative description of soil macrostructure by image analysis, *J. Soil Sci.* 38, 343-356, 1987.

Sahimi, M., *Applications of percolation theory*, Taylor and Francis, London, 1994.

Saucier, A. and J. Muller, Characterization of porous media with geometric multifractals, *Fractals*, 1, 894-903, 1993.

Schwartz, R.C., K.J. McInnes, A.S.R. Juo, and C.E. Cervantes, The vertical distribution of a dye tracer in layered soil, *Soil Sci.* 164, 561-573, 1999.

Solomon, S. G. Weisbuch, L. de Arcangelis, N. Jan, D. Stauffer, Social percolation models, *Physica A* 277, 239-247, 2000.

Stanley, H.E., J. S. Andrade Jr., S. Havlin, H.A. Makse, and B. Suki, Percolation phenomena: a broad-brush introduction with some recent applications to porous media, liquid water, and city growth, *Physica A* 266, 5-16, 1999.

Stauffer, D. and A. Aharony, *Introduction to percolation theory*, Taylor and Francis, London, 1992.

Stepanek, F., M. Marek, and P.M. Adler, Modeling capillary condensation hysteresis cycles in reconstructed porous media, *AIChE J.*, 45, 1901-1912, 1999.

Sukop, M.C., E. Perfect, and N.R.A. Bird, Impact of Homogeneous and Heterogeneous Algorithms on Water Retention in Simulated Prefractal Porous Media, submitted to *Wat. Resour. Res.*, 2001.

Sukop, M.C., G-J. van Dijk, E. Perfect, and W.K.P. van Loon, Percolation thresholds in 2-dimensional prefractal models of porous media, Submitted to *Transport in Porous Media*, 2001.

Turcotte, D.L., *Fractals and chaos in geology and geophysics*, Cambridge University Press, Cambridge, 1992.

Tyler, S. and S.W. Wheatcraft, Application of fractal mathematics to soil water retention estimation, *Soil Sci. Soc. Am. J.* 53, 987-996, 1989.

Tyler, S. and S.W. Wheatcraft, Fractal processes in soil water retention, *Water Resour. Res.*, 26, 1047-1054, 1990.

Tyler, S. and S.W. Wheatcraft, Reply, *Wat. Resour. Res.* 28, 603-604, 1992.

Yu, B-M. and K-L. Yao, Numerical evidence of the critical percolation probability $P_c = 1$ for site problems on Sierpiński gaskets, *J. Phys. A: Math. Gen* 21, 3269-3274, 1988a.

Yu, B-M. and K-L. Yao, Critical percolation probabilities for site problems on Sierpiński carpets, *Z. Phys. B -- Condensed Matter* 70, 209-212, 1988b.

Vita

Date and Place of Birth:

April 16, 1960; Newark, New Jersey, USA

Educational Institutions Attended and Degrees Awarded:

University of Kentucky, Lexington, Kentucky

Washington State University, Pullman, Washington; Master of Science

University of Wisconsin-Madison, Madison, Wisconsin

The Pennsylvania State University, University Park, Pennsylvania; Bachelor of Science

Mercyhurst College, Erie, Pennsylvania

Professional Positions Held:

Soil Scientist/Hydrogeologist, CH2M HILL Engineering, 1989 - 1997

Hydrogeologist, Donohue and Associates Engineering (now Earth Tech), 1984 - 1986

Scholastic and Professional Honors:

University of Kentucky Center for Computational Sciences Fellowship, 2000 -- 2001.

University of Kentucky Dissertation Enhancement Award, 1999

University of Kentucky Department of Agronomy Research Challenge Trust Fund Fellowship, 1997 -- 2000

American Water Resources Association -- Washington Section Fellowship Award 1988

California Registered Geologist No. 5615

California Certified Hydrogeologist No. 91

Kentucky Professional Geologist No. 2236

Professional Publications:

Refereed Publications

M.C. Sukop. 2000. Estimation of vertical concentration profiles from existing wells. *Ground Water*, 38, No. 6, 836-841.

E. Perfect and M.C. Sukop. 2001. Models to predict the dispersion of non-reactive solutes from pore characteristics. In Physical and Chemical Processes of Water and Solute Transport/Retention in Soils. D. Sparks and M. Selim. Eds. *Soil Sci. Soc. Am. Special Pub. No. 56*. Soil Science Society of America, Madison, Wisconsin.

M. Sukop and C.G. Cogger. 1992. Adsorption of Carbofuran, Metalaxyl, and Simazine: Koc evaluation and relation to soil transport. *J. Environ. Sci. Health B27(5)* 565-590.

Abstracts

M.C. Sukop and E. Perfect. 2000. Multifractal Behavior of Heterogeneous Fractal Porous Media. American Geophysical Union Fall Meeting, San Francisco.

E. Perfect and M.C. Sukop. 2000. Statistical Relations between Water Retention Parameters and Solute Dispersivity for Short, Undisturbed Soil Cores. American Geophysical Union Fall Meeting, San Francisco.

M. Sukop, G-J. van Dijk, E. Perfect, W.K.P van Loon. 2000. Percolation Thresholds in 2-Dimensional Prefractal Models of Porous Media. *Agronomy Abstracts*.

E. Perfect and M.C. Sukop. 1998. Models to predict the dispersion of non-reactive solutes from pore characteristics. *Agronomy Abstracts*

D.J. Mulla, M.C. Sukop, C. Cogger, and L.W. Getzin. 1989. Field Scale Variability: Effects on Pesticide Transport. *Agronomy Abstracts*

M. Sukop and C. Cogger. 1988. Spatial Structure of Pesticide Sorption Coefficients. *Agronomy Abstracts*

M. Sukop and C. Cogger. 1987. Pesticide Transport in Unsaturated Soil Columns. *Agronomy Abstracts*

M. Sukop. 1986. The Sandpack Dewatering Phenomenon in Slug Tests. American Water Resources Association --Wisconsin Section Annual Meeting, April 3 and 4.

Michael Sukop

March 21, 2001